Maria Luiza Onias Alves Pereira

Effect of Mo on the coarsening of Nb-precipitates

São Paulo

2014

Maria Luiza Onias Alves Pereira

Effect of Mo on the coarsening of Nb-precipitates

Trabalho de Formatura apresentado à Escola Politécnica da Universidade de São Paulo

Departamento de Engenharia Metalúrgica e de Materiais

Orientador: Prof. Dr. Hélio Goldenstein

São Paulo
2014

FICHA CATALOGRÁFICA

Pereira, Maria Luiza Onias Alves
Effect of Mo on the coarsening of Nb-precipitates / M.L.O.A. Pereira. -- São Paulo, 2014.
62 p.

Trabalho de Formatura - Escola Politécnica da Universidade de São Paulo. Departamento de Engenharia Metalúrgica e de Materiais.

1.Materiais metálicos 2.Precipitação 3.Nóbio 4.Molibdênio 5.Aços de alta resistência 6.Aços de baixa liga I.Universidade de São Paulo. Escola Politécnica. Departamento de Engenharia Metalúrgica e de Materiais II.t.

"Work as if you were to live a thousand years.
Pray as if you were to die tomorrow".
Benjamin Franklin

ACKNOWLEDGEMENTS

For this opportunity, I thank:

Professor Dr. Helio Goldenstein for accepting to be my supervisor and for all the help concerning the understanding of this subject.

Professor Dr. Mario González Ramirez for accepting in assisting this lecture and for all the help concerning the understanding of this subject.

Professor Dr. Eduardo Franco de Monlevade for accepting in assisting this lecture and for all the help concerning the understanding of this subject.

Professor Dr. Fernando Landgraf for all the lessons about the Graduation Project.

Dr. Ian Zuazo for the opportunity of the internship, for the work supervised.

Patrick Barges for sharing his office, for the help with the analyses, for the TEM and the precipitates analyses.

Professor Dr. Jeremie Bouquerel for his visit at the company.

Stéphan Joly for teaching how to do the thermal etching analyses and how to prepare its samples.

Coralie Magar for all the help with the dilatometer analyses.

RESUMO

Este trabalho apresenta um estudo preliminar da influência de Mo na precipitação de carbonetos de Nb que ocorre durante a formação da ferrita. Primeiramente, tratamentos cíclicos de austenitização, realizados para reduzir o grão austenítico inicial, provaram que isto foi possível somente após dois ciclos. Após este estudo, amostras contendo 0 Mo e 0,2 Mo foram submetidas ao tratamento de austenitização escolhido seguido por um longo tratamento isotérmico a 675 °C por 1h, 15h e 72h onde o comprimento dos precipitados foi medido. Os resultados preliminares mostram que o Mo retarda a formação da ferrita e que reduz o comprimento dos precipitados. O mecanismo de sua influência é discutido, porém não compreendido.

Palavras-chave: Precipitação, Nb, Mo, aços ARBL (aços de alta resistência e baixa liga), engrossamento de carbonitretos de Nb.

ABSTRACT

This work presents a preliminary study on the influence of Mo on Nb-precipitation occurring during ferrite from austenite formation. First, cyclic austenitization treatments, tested to reduce the starting austenite grain size, proved that this was possible after two cycles, but not further on. Then, samples containing 0 Mo and 0,2 Mo were submitted to the chosen austenitization treatment followed by long isothermal treatments at 675 °C for 1h, 15h and 72h where the lengthening of the precipitates was measured. The preliminary results show that Mo slows down the formation of ferrite and that it reduces the lengthening of the precipitates. The mechanism of its influence is discussed, but not understood so far.

Keywords: Precipitation, Nb, Mo, HSLA (high-strength low-alloy) steels, coarsening of Nb carbonitrides.

LIST OF FIGURES

LIST OF TABLES

LIST OF SYMBOLS

Nb	Niobium
Mo	Molybdenum
HSLA	High Strength Low Alloy
LSW	Lifshitz-Slyozov-Wagner
SEM	Scanning Electron Microscope
TEM	Transmission Electron Microscope
EDS	Energy Dispersive Spectroscopy

TABLE OF CONTENTS

I. Introduction

High-strength low-alloy steels (HSLA) steels have been widely used to improve the strength of materials by distributing fine carbides inside grains. These steels have been specially used in the automotive industry, where there is the need of reducing the weight of cars in order to decrease the fuel consumption [Park 2013].

This kind of steel presents high strength, excellent ductility and good weldability. With the introduction of alloying elements, these properties are improved. Chromium (Cr) and molybdenum (Mo) are used as such elements as they present a decreasing effect on the austenite transformation temperature [Lee 2002].

Mo is used in the present work as a carbide-forming element which would improve the resistance to coarsening. It is thought that it can influence the kinetics of ferrite formation and the stability of niobium-rich precipitates.

This work deals with the influence of Mo on niobium (Nb) precipitates, kinetics and size.

II. Objective

The aim of this project is to study the influence of alloying elements on the precipitation of Nb-rich particles in ferrite. This work focus on the influence of Mo on Nb precipitates.

This project is a part of a bigger project which studies the influence of alloying elements and transformation regimes on interphase precipitation of Nb in isothermal and continuous cooling conditions. Particular emphasis is placed on the effect of carbide-forming elements that could co-precipitate enhancing the resistance to coarsening.

III. Literature review

III.1. Precipitation

III.1.1. Introduction

Many important properties of alloys could be controlled by the presence of precipitated particles of a second phase, such as mechanical strength and corrosion resistance. These second phase particles result from the decomposition of a solid solution.

In order to a precipitate reaction take place, the alloy is first homogenized in the single-phase region at T_H, for instance, as shown in Figure 1, and then either

- cooled down slowly into the two-phase region (α + β). In this case, equilibrium can only be reached if the cooling rate is sufficiently low within a temperature range where there is still diffusion of the solute atoms. The precipitate volume fraction and the dispersion of the particles of the second phase can be controlled by the cooling rate.
- quenched to isothermal aging at a temperature within the two-phase region (α + β).

In both cases, thermodynamic equilibrium is reached if the supersaturation in the matrix Δc becomes zero.

$$\Delta c(t) = \bar{c} - c_\alpha^e \qquad \text{(Equation 1)}$$

where $\bar{c}(t)$ = mean matrix composition at time t with $\bar{c}(t = 0) \equiv c_0$

$c_\alpha^e(T)$ = equilibrium solubility limit, as seen in Figure 1 [Wagner 2001].

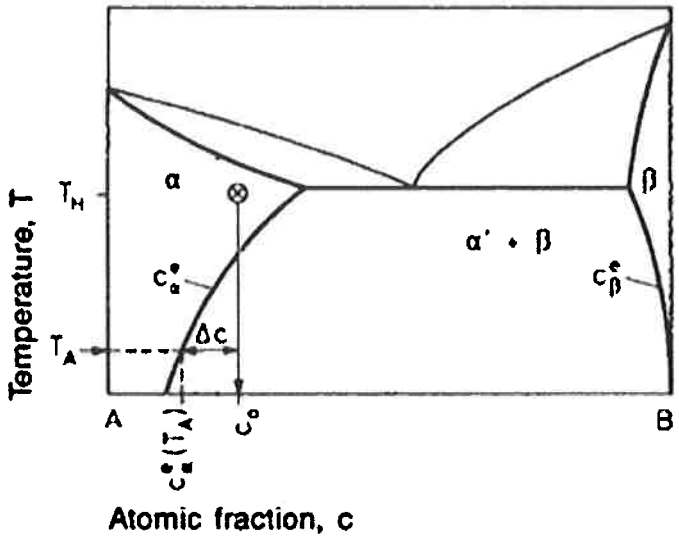

Figure 1 – Schematic phase diagram of a binary alloy [Wagner 2001].

III.1.2. Isothermal precipitation reaction

An isothermal precipitation reaction is characterized by an early stage during which an increasing number density of particles with a size distribution and a mean radius $\bar{R}$ is formed. In a precipitation reaction, there are three stages: nucleation, growth and coarsening.

In the earliest stages of the reaction, the parent phase α and the precipitate phase β share a common interface, that is, these two phases are coherent. During the earliest stages, $\bar{R}$ increases and the supersaturation Δc decreases slowly, which leads to the termination of the nucleation reaction of the new particles. The precipitate number density decreases due to the beginning of the coarsening reaction. During the coarsening reaction, the smaller particles redissolve, enabling the larger ones to grow and the supersaturation decreases towards zero [Wagner 2001].

The crystal structure of the equilibrium phase β precipitated is different from that of the parent phase α, which can lead to a coherent, semi-coherent or incoherent interface boundary, as seen in Figure 2 [Gleiter 1983 *apud.* Wagner 2001].

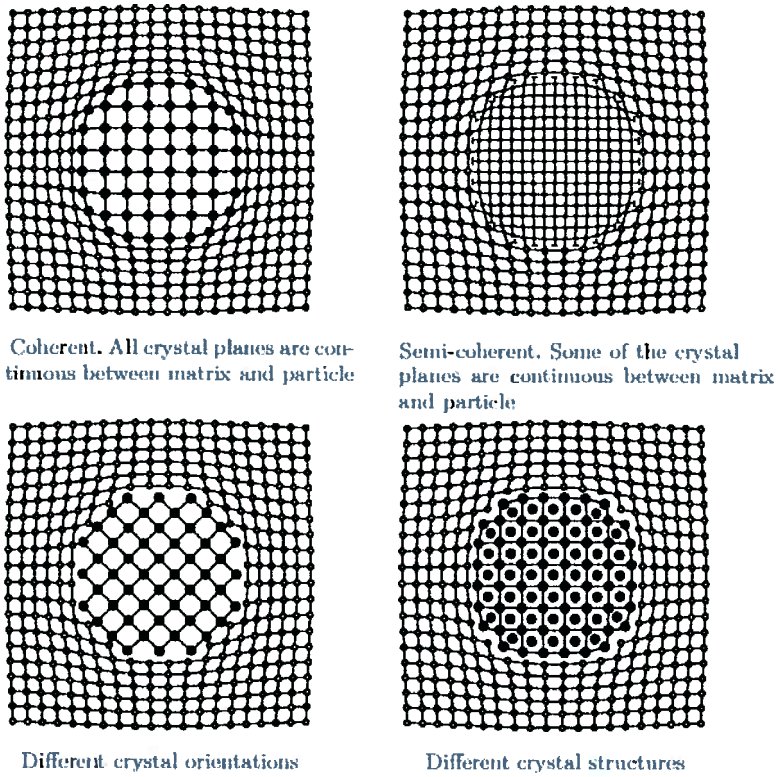

Figure 2 – Types of interface boundary between matrix and precipitate [Rösler 2006].

Since coherent interfaces have a lower energy than incoherent ones, a precipitate is usually coherent (or at least semi-coherent) during the early stages of nucleation and growth. The lattice parameter of a precipitate is usually different from that of its parent phase. Coherent nucleation usually happens at larger undercoolings or supersaturations and incoherent nucleation appears at smaller ones [Hornbogen 1967 *apud.* Wagner 2001].

III.1.3. Theory of diffusional growth

Precipitation proceeds via diffusional growth. Growth rates in diffusional transformations depend on:

- the mechanism by which the interface propagates through the parent lattice as the movement of coherent interfaces is different from that of incoherent ones. For example, movement of coherent or partially coherent interfaces must involve the co-ordinated shift of groups of atoms in order to preserve coherency, whereas an incoherent boundary may migrate through the capture of individual atoms;

- the orientation relationship between parent and product because the rate of growth of a crystal is different for different crystallographic directions;
- the rate of diffusion of the various atoms in both phases;
- the variation of solubility with curvature of the interface. Small particles of a phase present higher solubility than larger ones due to the difference in the radii of curvature of the interfaces.

In the diffusional growth of a single phase in a two-component system there is the transfer of atoms across an interface and also the re-distribution of the species, since the growing phase must have a different composition from the parent phase. The rate of growth depends upon the rate at which atoms are brought to, or removed from, the interface by diffusion and the rate at which they cross the interface.

Considering an isolated spherical particle of precipitate of radius R and solute concentration c_β growing in an infinitely large, homogeneous supersaturated solid solution of initial composition c_I, Figure 3 can be obtained. As the interface advances a small distance dR, the number of atoms captured by the precipitate per unit area of interface is $c_\beta \cdot dR$. Of these, $c_E \cdot dR$ were present at the interface. From Fick's first law, the diffusive flux at the interface is $D \cdot (\partial c/\partial r)_{r=R}$ where D is the value of the diffusivity of solute in the matrix at the concentration c_E and $(\partial c/\partial r)_{r=R}$ is the concentration gradient at the interface. The rate of growth is given by equation 2.

$$(c_\beta - c_E)\left(\frac{dR}{dt}\right) = D \cdot \left(\frac{\partial c}{\partial r}\right)_{r=R} \qquad \text{(Equation 2)}$$

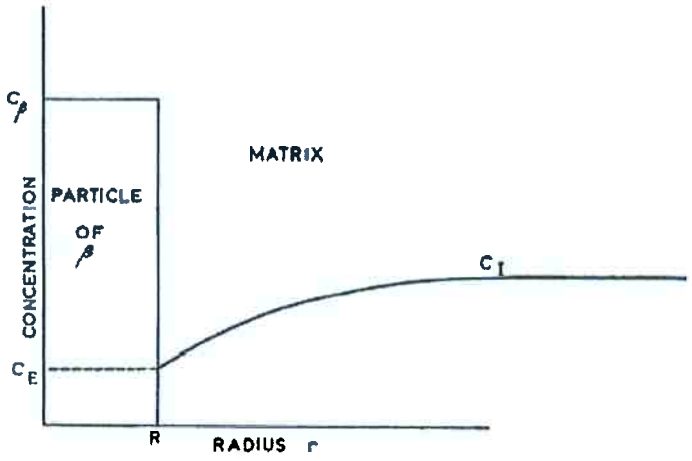

Figure 3 – The concentration of solute in and around a growing precipitate [Burke 1965].

In general, precipitation occurs on a number of particles each of which draws solute from the solution. This competition leads to a continuous decrease in the

matrix concentration from c_l and in the rate of growth of each particle. In the case of small supersaturations, the number of particles is small and so the distance of separation is large compared to the ultimate size [Burke 1965].

III.1.4. Thermodynamic considerations

It will be considered a binary alloy with N_A solvent atoms A and N_B solute atoms B with $N_A + N_B = N$.

The decomposition of a supersaturated single-phase alloy into a two-phase state occurring at constant temperature T and pressure p is initiated by a reduction of the Gibbs energy G with the enthalpy H. Thermodynamic equilibrium is reached when G of the system has reached a minimum [Gaskell 1983 *apud.* Wagner 2001].

$$G = H - TS \qquad \text{(Equation 3)}$$

$$H = U + pV \qquad \text{(Equation 4)}$$

$$\delta G_{T,p} = dU + pdV - TdS = 0 \qquad \text{(Equation 5)}$$

where S is the entropy, U is the internal energy and V is the volume.

For phase separation in solids, the term pdV can be neglected, so a good approximation for G is given by the Helmholtz energy F.

$$F = U - TS \qquad \text{(Equation 6)}$$

Equilibrium is achieved if F is minimized. At equilibrium, the chemical potentials $\mu_i^\alpha = \frac{\partial F^\alpha}{\partial n_i}$ and $\mu_i^\beta = \frac{\partial F^\beta}{\partial n_i}$ (i either A or B), where n is the number of particles, in the two phases are identical and the two phases have a common tangent to the associated free energy curves, as seen in Figure 4.

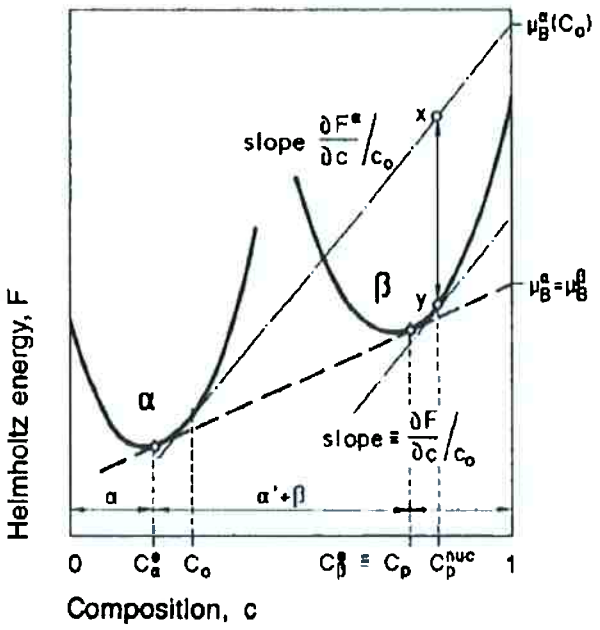

Figure 4 – Helmholtz energy F as a function of composition for a binary alloy [Wagner 2001].

III.1.5. Coarsening of precipitates: 'Ostwald ripening'

When a system containing a dispersed phase is annealed at a high temperature, the number of particles of the dispersed phase decreases while the average particle size increases. That is, during the coarsening process, the larger particles grow at the expense of the smaller ones. The driving force is the tendency to the reduction of the overall free energy by reducing the total area of internal interfaces. The coarsening reaction starts or becomes significant after the completion of the precipitation reaction, that is, when the solute content of the matrix approaches the Gibbs-Thomson solubility. The driving force for the precipitation is much larger than for coarsening.

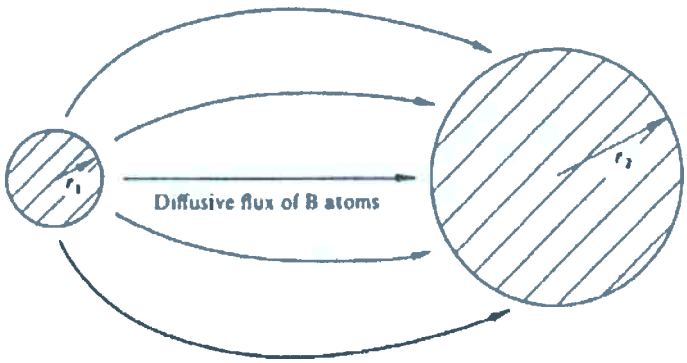

Figure 5 - Two spherical precipitates of radius r_1 and r_2. There is a diffusive flux from 1 to 2 [Martin 1997].

There is a diffusion of solute from regions close to small particles to regions around large ones, as seen in Figure 5, resulting that the concentration of solute in the solution in equilibrium with a precipitate is larger for a small particle of precipitate than for a large one; this can be seen from Figure 6. The tangents of Figure 6 show that the solubility of small particles $C_{\alpha(S)}$ is larger than that of large ones $C_{\alpha(L)}$. In a system containing mixed sizes, there is the diffusion of solute from regions around small particles to those close to large particles. The removal of solute from the solution near to small particles causes the dissolution of these small particles [Burke 1965].

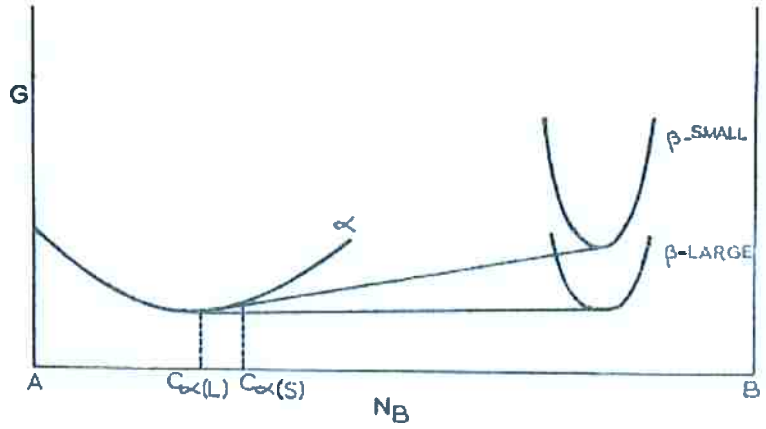

Figure 6 - The concentration of solute in a solution increases as the radius of curvature of the precipitate particles decreases [Burke 1965].

The solubility of a precipitate with an equilibrium shape must be constant all around it. As examples of non-spherical equilibrium shapes, there are particles with plate-like or rod-like morphologies, which provide more barriers for dislocation glide than precipitates of equivalent volume fraction with spherical shape. For fcc copper precipitates in a bcc iron matrix, the equilibrium shape was rod with curved ends, as shown in Figure 7 [Speich 1965].

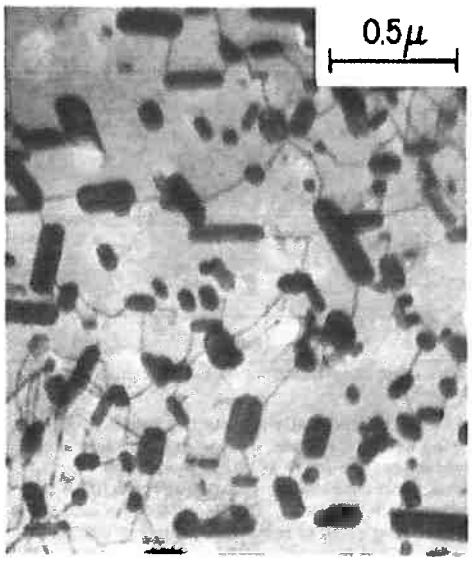

Figure 7 – Copper precipitate in a Fe-4.0 wt % Cu alloy aged 300h, 680 °C [Speich 1965].

In the analysis of Greenwood [Greenwood 1969] and LSW (Lifshitz-Slyozov-Wagner) [Lifshitz 1961, Wagner 1961 *apud.* Martin 1997], it was shown that in an array of particles, all particles smaller than the average particle radius $\bar{r}$ will shrink and the rate of shrinkage increases rapidly as $r/\bar{r}$ approaches to zero. Also, all particles larger than $\bar{r}$ will grow. So, as time goes on, the dispersion becomes coarser and the mean particles radius $\bar{r}$ increases with time. The LSW equation for the coarsening rate, which considers a negligible volume fraction of particles and no elastic interaction between particles, is shown in equation 7.

$$\bar{r}_t^3 - \bar{r}_0^3 = 8D\sigma N_\alpha V_m t/9RT \qquad \text{(Equation 7)}$$

where $\bar{r}$ is the mean radius of a distribution of spherical particles, D is the diffusion coefficient, σ is the interfacial energy, N_α is the number of moles of α, V_m is the molar volume, t is time, R is the gas constant and T is the temperature.

The analysis made by Fang and Patterson studied the effect of different initial particle size distribution on coarsening and resulted that the rate of coarsening was controlled by the size distribution: narrow distributions coarsened slowly and wide distributions coarsened quickly [Fang 1993 *apud.* Martin 1997]. The particle size distribution of the LSW model may only be used in real-life problems with experiments from initially very narrow distributions where particles of a size greater than $1.5\bar{r}$ are not present. Most two-phase metallic microstructures are made from precipitation that always generates wide size distributions [Martin 1997].

In a ternary or in higher order alloys, the coarsening rate will be modified by the addition of an excess of the faster diffusing component [Bhattacharya 1972]. In the study of coarsening of carbides in steel, where the interstitial diffusion of carbon is very much faster than that of the binary iron carbide Fe_3C, it was seen that coarsening will be significantly slowed for ternary elements with a low diffusion coefficient in the matrix and when there is a high concentration of the ternary element in solution in the matrix [Bjorklund 1972 *apud.* Martin 1997]. Therefore, multiple element addition will usually retard coarsening.

III.2. HSLA steels

High strength low alloy (HSLA) steels were developed in the 1960's when microalloy additions and thermomechanical processing have been combined to attain a set of desirable mechanical properties through microstructural control. This kind of steel is used in construction, transportation and pipeline applications.

HSLA steels have a yield strength level greater than that of mild steel and are predominantly low in carbon (0,05 to 0,15 weight percent), alloyed with small quantities of carbide-forming elements such as niobium, titanium and vanadium (0,10 weight percent or less) [Lechuk 2000]. These micro-alloying elements improve the properties, acting, mainly, on the austenite grain size and, consequently, on the recrystallization and on the hardness of the matrix by a hardening effect [Hulka].

III.2.1. Microstructures

a) Ferrite + pearlite

It has a good combination of high yield strength (σy) and low impact transition temperatures (ITT); the latter indicates the resistance to brittle cleavage fracture. Several microstructural parameters are associated to yield strength, but the main parameter is the refinement of the ferrite grain size as it improves the strength and it is the only strengthening mechanism which decreases the ITT, as shown in Figure 8 [Pickering 1992 *apud.* Serafim da Silva 2013].

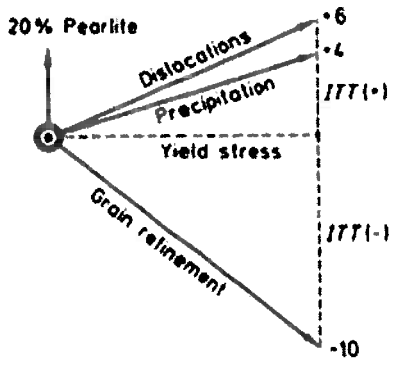

Figure 8 - Strengthening mechanisms in HSLA steels comprising ferrite-pearlite microstructures, showing their effects on the change in impact transition temperatures. The ratios indicate the change in the ITT for a yield strength (σy) increase of 15 MPa. [Pickering 1992].

Figure 8 shows that the dislocation strengthening causes a more negative effect on the ITT than the precipitation strengthening, the latter is more recommended. The pearlite increases the ITT so its presence must be avoided. The ITT is also influenced by compositional factors such as the use of aluminum and manganese. They are favorable to the toughness (decrease of the ITT) as it can be seen in Figure 9 [Pickering 1992 *apud.* Serafim da Silva 2013].

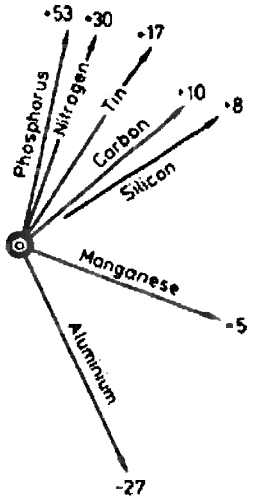

Figure 9 - Compositional factors in HSLA steels comprising ferrite-pearlite microstructures, showing their effects on the change in impact transition temperatures. The ratios indicate the change in the ITT for a yield strength (σy) increase of 15 MPa. [Pickering 1992].

b) Acicular ferrite

A new microstructure was developed by lowering the carbon content because the latter improves the toughness. The microstructure consists of a matrix known as acicular ferrite which contains small islands of martensite and residual austenite, as seen in Figure 10. This microstructure is highly sub-structured and contains high dislocation density. The solid solution strengthening effects are more significant in this microstructure than in the ferrite + pearlite microstructure [Keown 1985 *apud*. Serafim da Silva 2013].

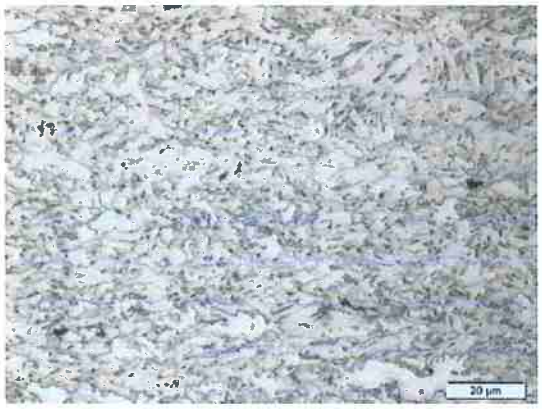

Figure 10 - Example of Acicular Ferrite microstructure (0,059wt.%C, 1,54 wt.%Mn,0,030 wt.%Nb) [Keown 1985].

c) Dual-phase steels

The microstructure of dual-phase steels, shown in Figure 11, consists of ferrite containing islands of martensite-austenite, the M-A constituent, and small amounts of bainite may also appear. It is characterized by higher tensile strength and a continuous yielding behavior. This type of microstructure requires a high rate of nucleation of austenite during intercritical annealing and a slow rate of growth of austenite to produce small particles of the M-A constituent [Jia-ling 1988].

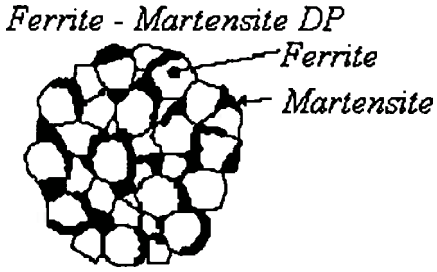

Figure 11 - Example of ferrite-martensite microstructure [Jia-ling 1988].

III.3. Mo influence

The Fe-Mo phase diagram can be seen in Figure 12 and it shows which phases are to be expected at equilibrium for different combinations of molybdenum content and temperature.

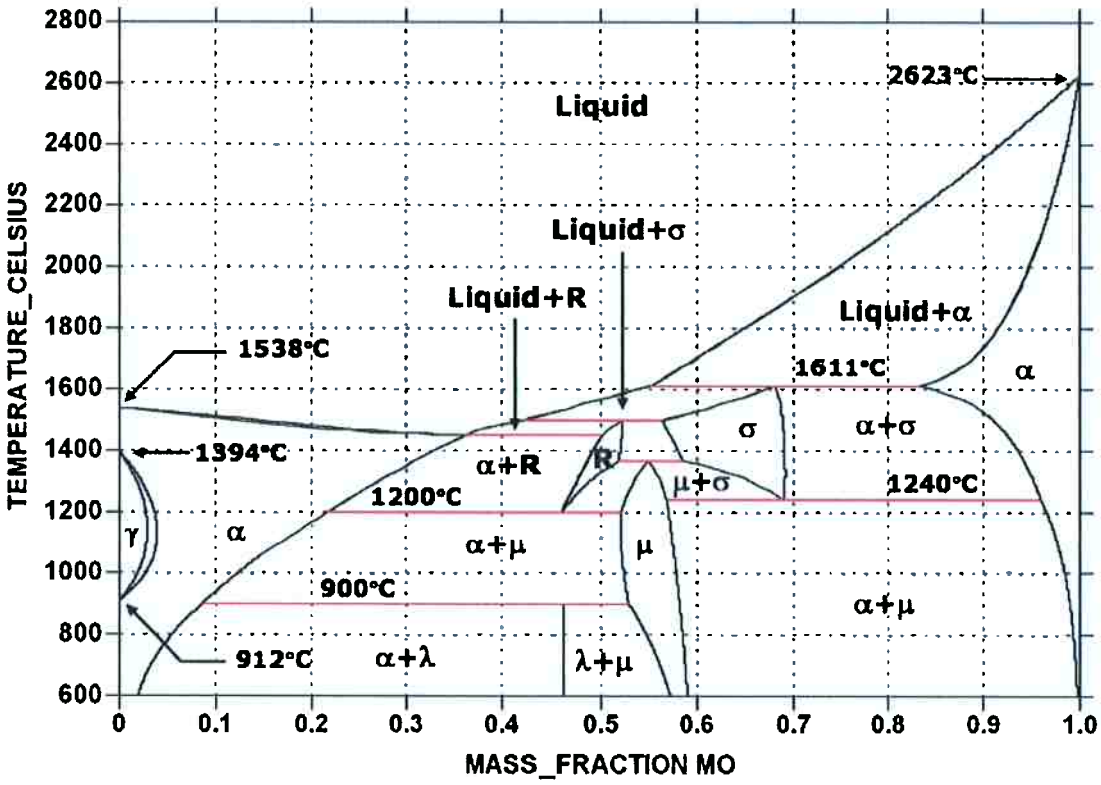

Figure 12 – The Fe-Mo phase diagram was calculated with Thermo-Calc®, coupled with SBIN2 thermodynamic database [Calphad].

Molybdenum affects the microalloy precipitate evolution during processing in ferrite and austenite. Precipitation of molybdenum carbide is widely used to increase strength at elevated temperatures in high-speed or tool steel applications. Some of its characteristics may be found as follows:

a) is incorporated into microalloy precipitates during precipitation and low-temperature coarsening [Akben 1983 *apud.* Enloe 2012].
b) reduces thermodynamic stability of complex carbonitrides at austenitic temperatures [Houghton 1982 *apud.* Enloe 2012].
c) reduces energetic barriers at the early stages of nucleation [Lee 2002].
d) beneficial reduction in Nb diffusivity in austenite and ferrite.
e) segregates to the carbonitride-ferrite matrix interface [Uemori 1994 *apud.* Enloe 2012].
f) slows the incorporation of Nb into the carbonitride or reduce the interfacial energy, thus reducing the coarsening rate [Speer 2010 *apud.* Enloe 2012].

In Mo containing HSLA steels, the Mo is usually added to control the austenite decomposition kinetics and it has been observed in relatively fine complex microalloy carbonitride precipitates that form in ferrite and to a lesser extent in austenite. Molybdenum incorporation is unlikely in the austenitic regime due to the high solubility of MoC in austenite [Pavlina 2012]. Upon cooling and transformation from austenite to ferrite, Mo incorporation into the precipitates is expected to become more favorable, so the regions of the precipitate that grew at lower temperatures have higher concentrations of Mo. Consequently, Mo incorporation is expected to be significant in the ferrite regime. Substantial incorporation of Mo into the carbonitride precipitates likely occurs during precipitate nucleation and/or growth in ferrite. Mo also inhibits Nb carbonitride coarsening in fire-resistant steels by segregating at the matrix/precipitate interface.

The studies of Enloe et al suggest that Mo is incorporated into the precipitates during cooling from hot-rolling and then partitions back into austenite during hold at elevated temperature. The same study showed that smaller particles, formed at lower temperatures, have a higher Mo-enrichment while larger particles, formed at higher temperatures, are less Mo-enriched. In this study there was the comparison of two samples which had a similar amount of Mo, but different amounts of Niobium. The sample which presented higher Nb concentration showed increased precipitate number density and it was noticed the incorporation of Mo in Nb-rich precipitates in austenite at 900°C [Enloe 2012].

Due to the demand for high strength steels in the automobile industry, several studies were made about the strengthening mechanism and high-strength low-alloy (HSLA) steels have been widely used. Park *et al* compared the precipitation

hardening of different combination of microalloying elements and the steel with Nb-Mo was the one with the best results. In this work, it was studied the strengthening of HSLA steels and it was seen that smaller precipitate size generally leads to the increase in strength of HSLA steels by increasing the distribution density of the precipitation. As an example, although Ti in HSLA is more efficient for strengthening than V or Nb, steel with Nb-Mo presented higher yield and tensile strengths than steel with Ti-Mo. This is mainly because of the precipitation hardening contribution which is originated from the decrease in precipitate size [Park 2013].

III.4. Nb precipitation

Nb influences the mechanical properties of steels as it refines the grain and it lowers the γ to α transition temperature (Ar3). Grain refinement increases strength, toughness and ductility. The grain refining effect of Nb is mainly due to delaying or preventing recrystallisation in the last hot-forming steps. Flattened grains and a high dislocation density of the austenite enhance ferrite nucleation. By lowering the γ to α transformation temperature, Nb simultaneously enhances the ferrite nucleation rate and reduces the grain growth rate. The combined effect leads to a particularly fine-grained transformation structure [Klinkenberg 2007].

Nb has a high affinity for both carbon and nitrogen when added to steels; Nb carbide and nitride are mutually soluble, forming a cubic-type crystal structure. Since steels usually contain both carbon and nitrogen, it is assumed that a carbonitride is formed, rather than a pure carbide or nitride or both [Lechuk 2000].

The equilibrium diagrams of Nb-C and Nb-N are shown in Figure 13. These systems show an M_2I phase, where M and I represent the metal and the interstitial atom, respectively [Park 1991].

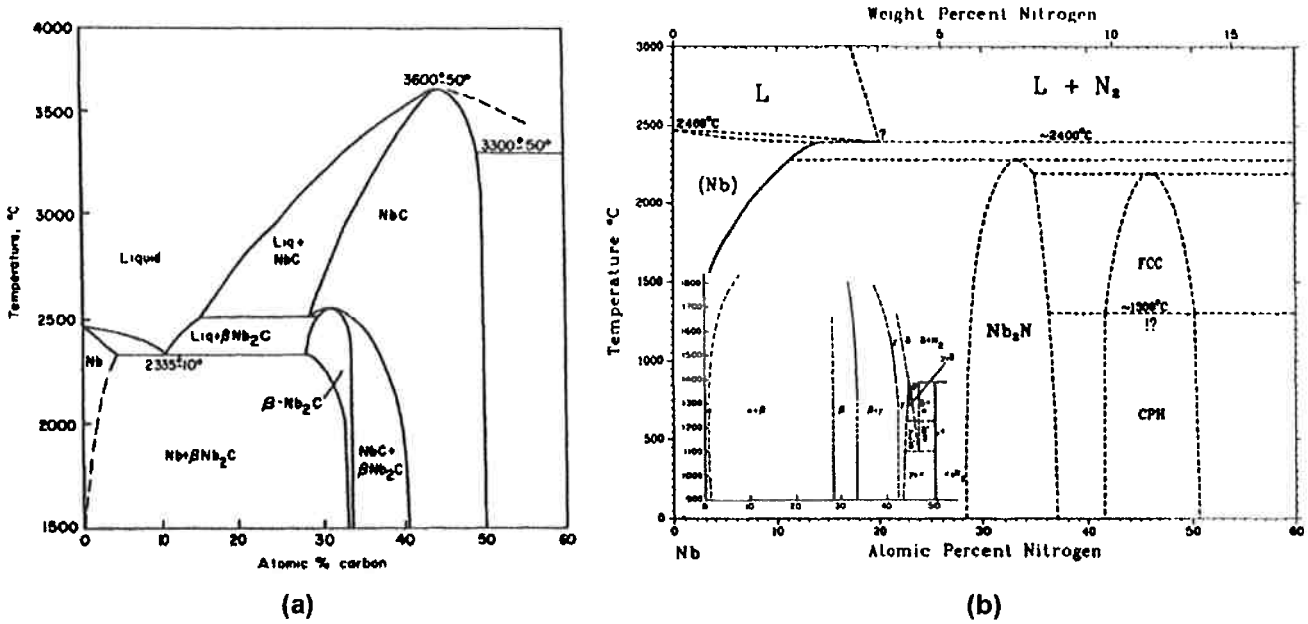

(a) (b)

Figure 13 – Phase diagrams for (a) Nb-C and (b) Nb-N [Park 1991].

Solubility data from literature is shown in Figure 14.

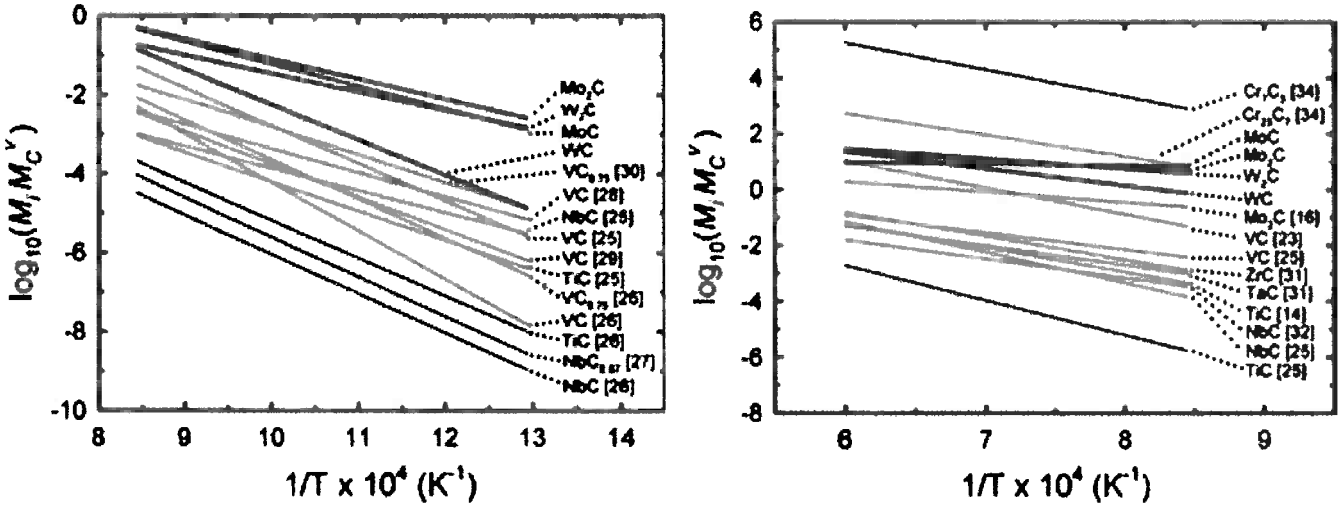

(a) (b)

Figure 14 –Comparison of Mo2C and NbC solubility products in (a) ferrite (773–1184 K) and in (b) austenite (1184–1666 K) with other carbide solubility products [Pavlina 2012].

Most commercial HSLA steels contain at least two carbide and/or nitride-forming microalloy additions. Many of these precipitates, such as Nb(CN) and Ti(CN), are completely intersoluble, allowing for the formation of complex carbonitrides having a wide range of composition and thermodynamic properties.

Precipitates formed in austenite are subjected to a relatively fast coarsening and lose part of their potential efficiency as ferrite strengtheners. Precipitation of Nb

in ferrite is expected to be significantly finer and contribute to increase the tensile properties [Altuna 2009].

In the work of *Yu et al.*, it was studied the role of Nb and Mo as carbide-forming elements. It was seen that there is a fine grain structure and a strong delay of γ/α transformation in addition to an increase in toughness and strength properties when both elements work together [Yu 2013].

IV. Materials and methods

This is an ongoing project, which started one year and a half before this text was written, and several heat treatments were already determined.

A temperature for ferrite formation was determined in which a compromise between the presence of allotriomorphic ferrite and reasonable kinetics was obtained. This temperature was 675°C for an austenitization temperature of 1200°C. The latter was chosen in order to put the maximum amount of microalloyed elements into solution.

The samples of HSLA steels used in this work are presented on Table 1. A complete composition of theses samples can be seen in Annex 1.

Table 1 – Composition of the alloys studied.

(wt%)	C	Nb	Mo	Mn
0 Mo	0,0530	0,1000	0,0048	1,5000
0,1 Mo	0,0550	0,1100	0,1200	1,5000
0,2 Mo	0,0560	0,1000	0,2100	1,5000
0,4 Mo	0,0550	0,1100	0,4000	1,5418

IV.1. Grain size study

As the austenitization temperature chosen was 1200 °C, the starting grain size was going to be large and had a negative effect on the kinetics of ferrite formation. Therefore, a preliminary study was performed to assess the influence of cyclic treatments on austenite grain size reduction. To do so, three cylindrical samples of 0,1 Mo of 5 mm in diameter and 10 mm in length were tested in a dilatometer using three different cycles each:

i. heated at 10 °C/s until 1200 °C, where they were held for 5 minutes and then helium quench;
ii. cycle i plus heated at 50 °C/s until 1200 °C, where they were held for 1 minute and then helium quench;
iii. cycle ii plus heated at 50 °C/s until 1200 °C, where they were held for 1 minute and then helium quench.

Those cycles are represented on Figure 15.

It is known that the austenite grain size, when transformed from a fully martensitic structure, will be smaller than the parent austenitic grain size of that martensite (at the same austenitization temperature). Therefore, the heat treatments have a common 1200 °C temperature, but three different austenitization times were performed on the 0,1 Mo sample.

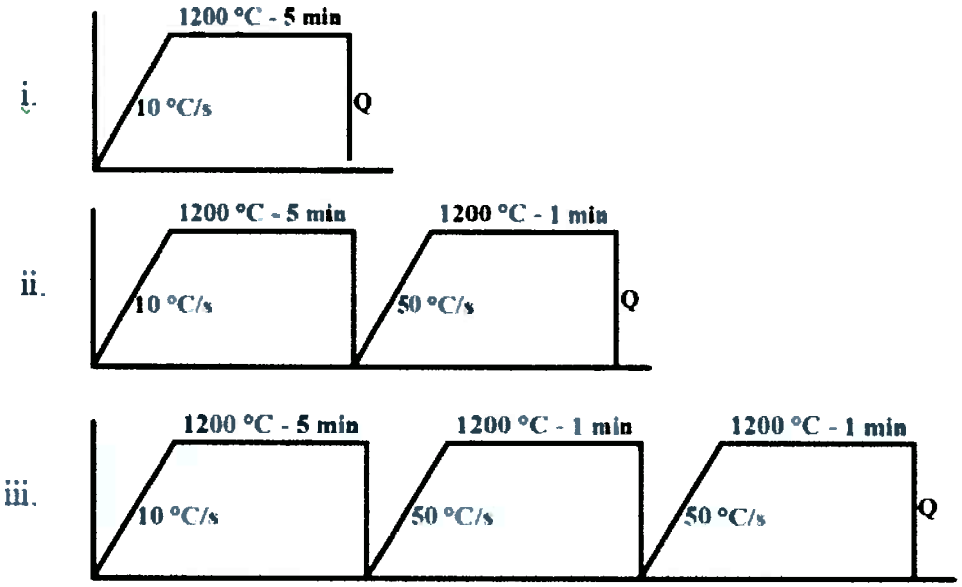

Figure 15 – Heat treatments used to analyze the grain size: i. heated at 10 °C/s until 1200 °C, where they stood for 5 minutes and then quench; ii. cycle i plus heated at 50 °C/s until 1200 °C, where they stood for 1 minute and then quench; iii. cycle ii plus heated at 50 °C/s until 1200 °C, where they stood for 1 minute and then quench.

0,1 Mo samples were chosen as considered representative of all samples. To analyze the effect on grain size, the technique of the thermal etching was used. The thermal etching method consists in revealing the austenite grain boundaries in a prepolished sample by the formation of grooves at the intersections of austenite grain boundaries with the polished surface when the steel is exposed to a high temperature in an inert atmosphere. These grooves decorate the austenite grain boundaries and make them visible at room temperature in an optical microscope [García de Andrés 2003].

Firstly, the samples were metallographic prepared, that is, they were mounted and polished using standard metallographic techniques, finishing with 1-μm diamond paste. This preparation occurred before the last cycle with quench, the

thermal etching, as samples tested after thermal etching do not require metallographic preparation after heat treatment. After being polished, they were unmounted and then submitted to the thermal etching. The thermocouples were welded at the opposite side of the polished sample. This preparation is presented on Figure 16.

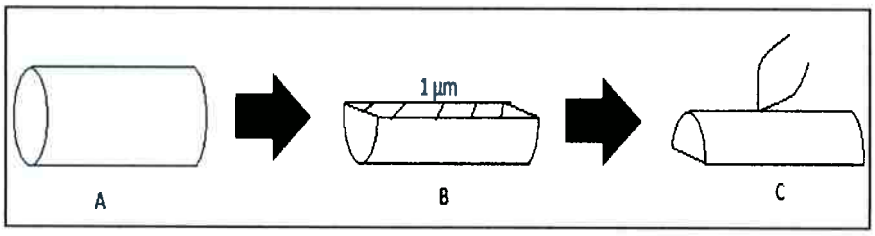

Figure 16 - Preparation of the samples for the thermal etching test with a 0,1 Mo sample. In this treatment, a polished surface is subjected to a thermal treatment under good vacuum conditions.

To measure the grain size, the Aphelion® software was used. An example of the measurement of the grain size can be seen in Figure 17.

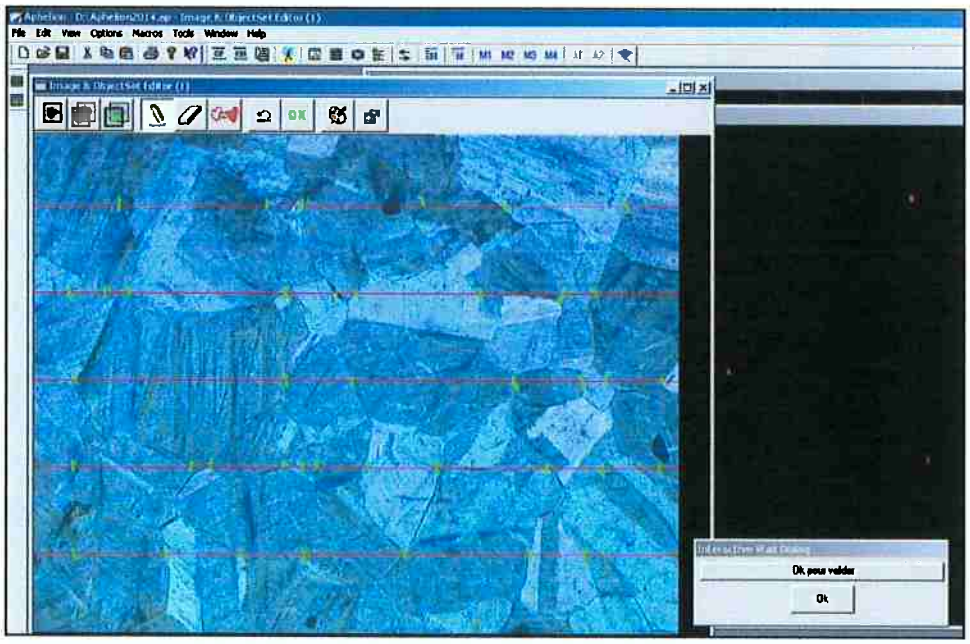

Figure 17 – Example of grain size measurement at the Aphelion® software for a 0,1 Mo sample with a treatment of 5' + 1' (cycle ii).

IV.2. Study of the influence of Mo

Cylindrical 0 Mo and 0,2 Mo samples of 5 mm in diameter and 10 mm in length were submitted to dilatometer cycles. These cycles consisted first of an austenitization step (cyclic treatment) using type ii cycle (see item II.3.1) and then the samples were cooled down to 675 °C and held for 1 h, 15 h or 30 h. An example of this cycle can be seen in Figure 18. For the 30 hour-treatments, vacuum was maintained during holding. To do the vacuum on this dilatometer first the vacuum button was pushed and then, when it reached a good vacuum, it was turned off and a little Helium was turned on. This good vacuum depended if the analysis was of thermal etching, which needs a good vacuum, or isothermal treatment, in which vacuum is needed, but not so strong as in thermal etching.

After the dilatometer analysis, the samples were cut at the middle where the thermocouples are and then they were metallographic prepared, that is, they were mounted and polished using standard metallographic techniques, finishing with 1-μm diamond paste and etched with Nital 2 % (2 mL of HNO_3 in 98 mL of ethanol).

0,4 Mo sample was also treated for 1h at 675 °C on the dilatometer.

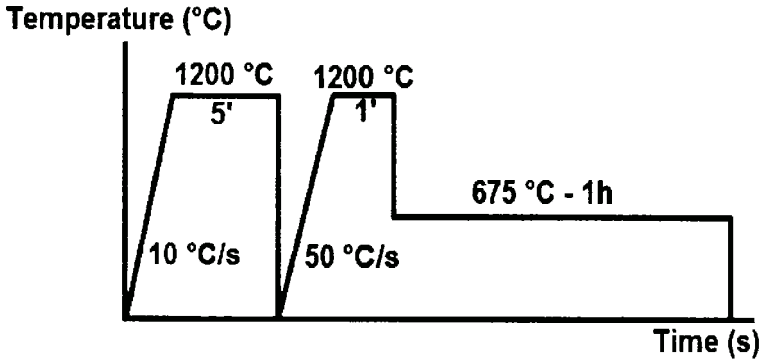

Figure 18 – Dilatometer cycle in which the samples were submitted.

Preliminary results showed that the samples suffered decarburization. In order to avoid decarburization, it was decided to nickel-coat the samples and to protect even more the samples and prevent decarburization, instead of performing the long cycles on the dilatometer, the samples were submitted to a 1 hour-cycle at the dilatometer at 675 °C (including the austenitization step) and then they were placed inside ampoules in vacuum and treated in the Nabertherm® furnace at 675

°C. With this new procedure, it was possible to perform even longer treatments, as for 72 hours.

In order to better analyze the results, a sample of 0 Mo was passed through a 1-hour treatment, quenched and then reheated to 675 °C for another 1h.

So after the heat treatments, the samples were metallographic prepared as already explained. The samples that stood for 72h at 675 °C were etched with Nital 2 % (2 mL of HNO_3 in 98 mL of ethanol) and Picral (4 g of picric acid in 100 mL of ethanol) to reveal the carbides.

To better understand the microstructures obtained, micro-hardness tests were made on the 0 Mo and on the 0,2 Mo samples that stood for 15h at 675 °C.

The objective of this investigation is to study the influence of Mo on precipitation, therefore the precipitates were extracted by carbon replicas to be observed in the Transmission Electron Microscope (TEM). First, after all the metallographic preparation, including the chemical etching, a carbon replica was deposited on the surface and then it was etched with a solution to remove the carbon replica. This solution consisted of 20 % nitric acid in water. After this preparation, which can be seen in Figure 19, the replicas were observed in the TEM, in order to study the precipitates evolution. The TEM images were transferred to the Aphelion® software to measure the precipitates size.

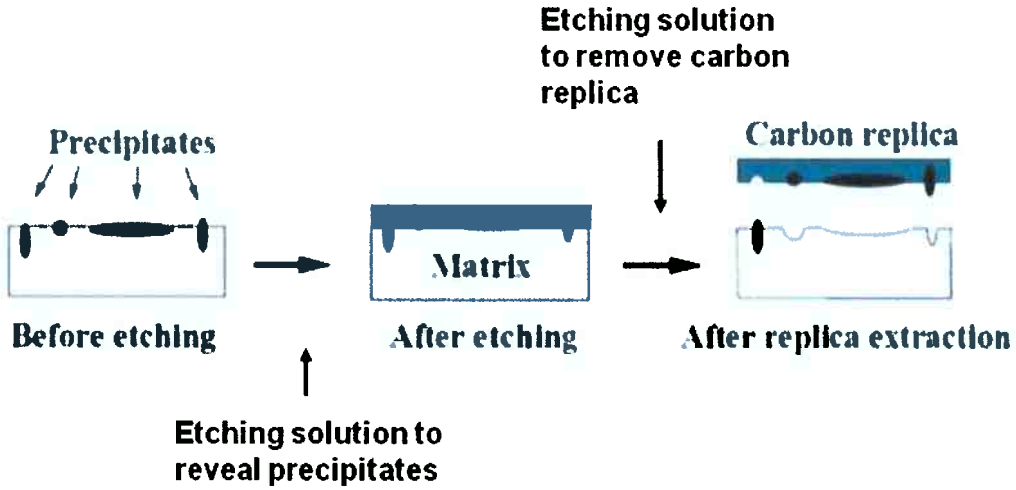

Figure 19 – Preparation of the carbon replica.

IV.3. Techniques

IV.3.1. Dilatometry

Dilatometry is one of the most powerful techniques for the study of transformations in steels because it permits the real-time monitoring of the extent of reaction in terms of dimensional changes due to transformation [Takahashi 1989]. The dilatometric method utilizes transformation strains and thermal strains. Raw Data is given usually in the form of curves of dimension against time and temperature [Bhadeshia 2000].

In interpreting the experimental data, it is usually assumed that during isothermal reaction, the dimensional change observed is proportional to the volume fraction of transformation and it is assumed that the point where dimensions cease to change represents 100% of transformation. When reaction ceases before the parent phase has completely transformed, it is useful to be able to calculate the volume fraction of product phase that has been obtained [Takahashi 1989].

A sample placed in the dilatometer measuring unit is heated in a temperature homogeneous zone by furnace. The volume change is measured in one direction as displacement of push-rod caused by elongation or contraction of the sample. The temperature of the sample is measured by a thermocouple [Netzch 2005]. An example of the measuring unit can be seen in Figure 20.

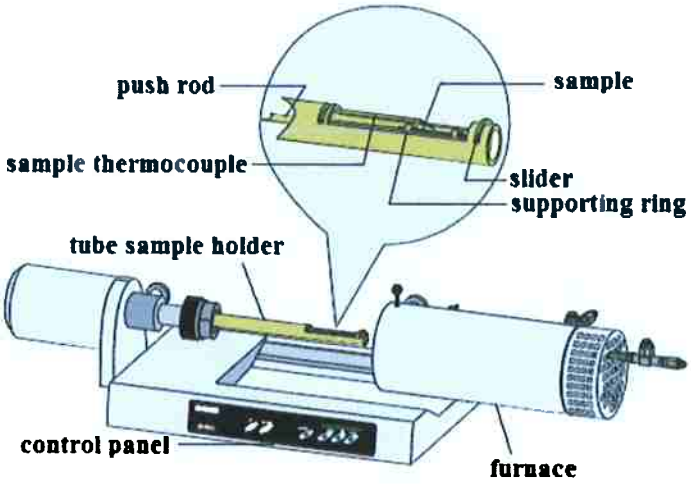

Figure 20 - Example of measuring unit [Netzch 2005].

The sample may be under protective atmosphere or vacuum. Temperature or time of volume change are stored as separated data values and are showed as

graphs by the computer. The shape of dilatometric curve depends on the process settings (mainly the heating or cooling rate) and the composition and homogeneity of the sample [Tariq 2010]. Schematic examples of dilatometric curves are shown in Figure 21.

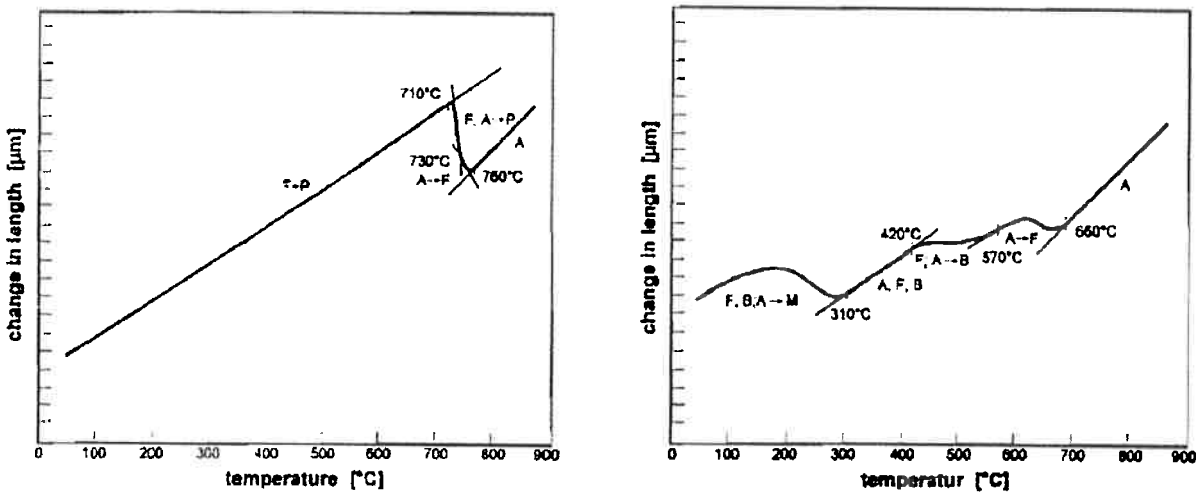

Figure 21 – Length-temperature curves of a (a) quenched and (b) tempered steels (schematic) [Stahl-Eisen 1998].

Dilatometric curves of steel can be divided into regions according to the shape, linear parts and transformational regions. By heating a ferritic microstructure, proportional increase of length is observed at first because of the linear thermal expansion of the sample. The transformation is observed in the dilatometric curve as sudden change in the curve shape. In steel, A_{c1} temperature is observed as sudden decrease of volume because volume of austenite is lower than volume of ferrite at the same temperature. When all α-ferrite is transformed, dilatometric curve stops to decrease. This local minimum is A_{c3} temperature and the sample is now fully austenitic. Above A_{c3}, the sample is fully austenitic and the volume increases again because of linear thermal expansion. As the austenite starts to transform into δ-ferrite, sudden increase of volume is observed [Köver 2012].

Dilatometry may be used to determine the temperature of phase transformation, the ratio of phases in two-phase region at any temperature and coefficient of linear thermal expansion. Quenching and deformation dilatometer can be used to determine the influence of high heating and cooling rates and of applied load on the kinetics of solid state phase transformations [Bhadeshia 2000].

IV.3.2. SEM

The scanning electron microscope (SEM) is a microscope that uses electrons instead of light to form an image. It uses a focused beam of high-energy electrons to generate a variety of signals at the surface of solid specimens [Goldstein 2003].

Electrons are produced at the top of the column, accelerated down and passed through a combination of lenses and openings to produce a focused beam of electrons which hits the surface of the sample. The sample is mounted on a stage in the chamber area and both the column and the chamber are evacuated by a combination of pumps. The position of the electron beam on the sample is controlled by scan coils situated above the objective lens. As a result of the electron-sample interaction, a number of signals are produced. These signals are then detected by appropriate detectors. The signals that derive from electron-sample interactions reveal information about the sample such as external morphology (texture), chemical composition and crystalline structure and orientation. A scheme of the SEM can be seen in Figure 22 [NanoScience].

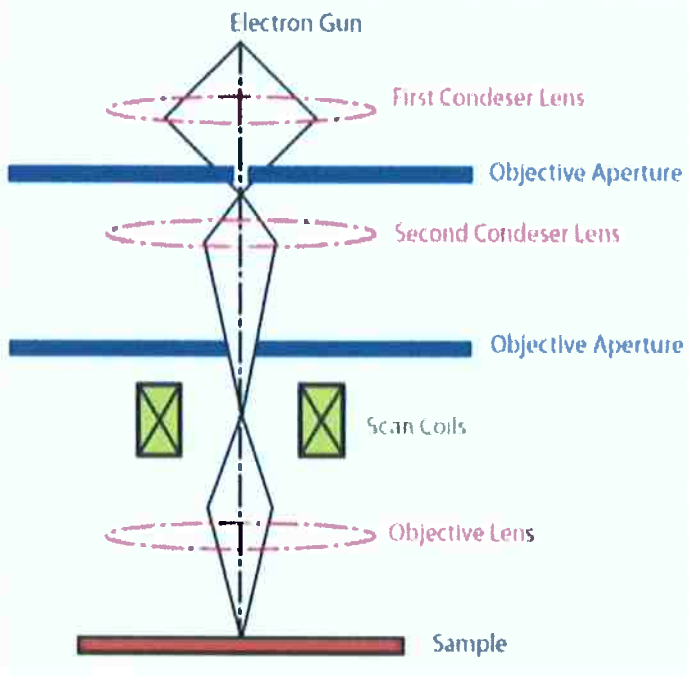

Figure 22 – Schematic drawing of a SEM [NanoScience].

Accelerated electrons in an SEM carry significant amounts of kinetic energy, and this energy is dissipated as a variety of signals produced by electron-sample interactions. These signals consist of secondary electrons (that produce SEM images), backscattered electrons, diffracted backscattered electrons (that are used to determine crystal structures and orientations of minerals), photons (characteristic X-rays that are used for elemental analysis and continuum X-rays), visible light (cathodoluminescence) and heat. Secondary electrons and backscattered electrons are commonly used for imaging samples: secondary electrons are most valuable for showing morphology and topography on samples and backscattered electrons are most valuable for illustrating contrasts in composition in multiphase samples [Goldstein 2003].

IV.3.3. TEM

Compared to a SEM, a TEM (Transmission Electron Microscope) has better spatial resolution and is capable of additional analytical measurements, but requires significantly more sample preparation.

A TEM produces a high-resolution, black and white image from the interaction that takes place between prepared samples and energetic electrons in the vacuum chamber. Air needs to be pumped out of the vacuum chamber, creating a space where electrons are able to move. The electrons then pass through multiple electromagnetic lenses. The beam passes through these lenses, down the column, makes contact with the screen where the electrons are converted to light and form an image. The lighter areas of the image represent the places where a greater number of electrons were able to pass through the sample and the darker areas reflect the dense areas of the object where fewer electrons were passed through. These differences provide information on the structure, texture, shape and size of the sample. A scheme of a TEM and its comparison with a light microscope and with a SEM can be seen in Figure 23.

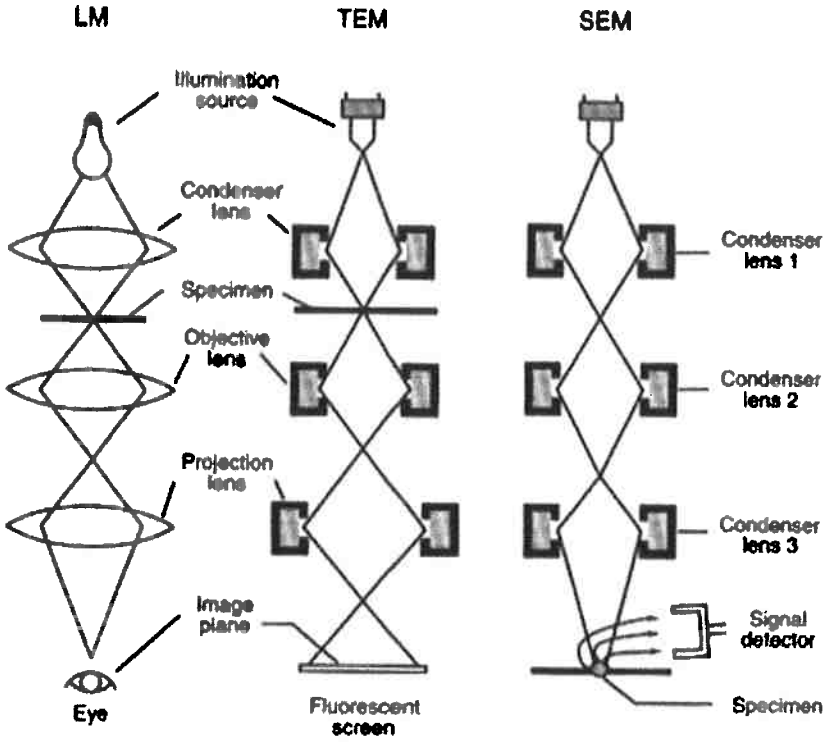

Figure 23 – Comparison of the functioning of a light microscope, a TEM and a SEM [Central Microscopy].

To obtain a TEM analysis, samples need to have certain properties. They need to be sliced thin enough for electrons to pass through, a property known as electron transparency [Microscope Master].

V. Results and Discussion

V.1. Grain size study

The results of the grain size measurement using 0,1 Mo sample can be seen in Table 2. In order to improve kinetics, a smaller grain size is needed.

Table 2 – Results of the grain size measurement for each heat treatment.

	Grain size (μm)
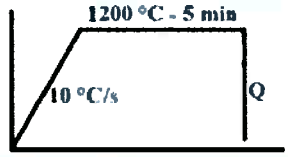	162,6 ± 18,5
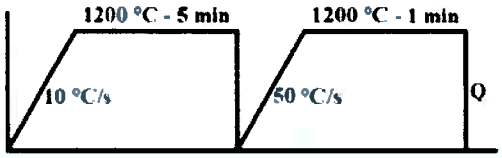	114,9 ± 7,5
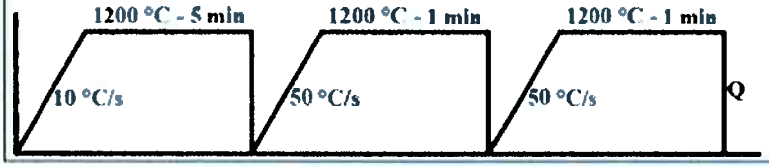	112,2 ± 6,4

By analyzing the results on Table 2, it is possible to see that the difference in grain size between the first and second cycle is interesting, but not that large and no effect was observed by performing a third cycle. These results are in accordance with [Furuhara 2008] that showed that the effect is very important with a second cycle, but that the austenite grain size is almost stabilized after a third cycle.

In order to start with the smallest austenite grain size so that the kinetics should be better, but not tested yet, the samples in this study have been treated using two cycles, that is, cycle ii.

V.2. Study of the influence of Mo

V.2.1. Decarburization

After the first analyses on the dilatometer of 1h, 15h and 30h cycles, by observation on optical microscope, it was seen that the samples suffered decarburization. It occurred during treatment at 1200°C, but mainly during isothermal holding at 675°C. Figure 24 shows the microstructures near the center of the samples and the advancement of decarburization in both alloys as a function of time during isothermal treatment at 675°C.

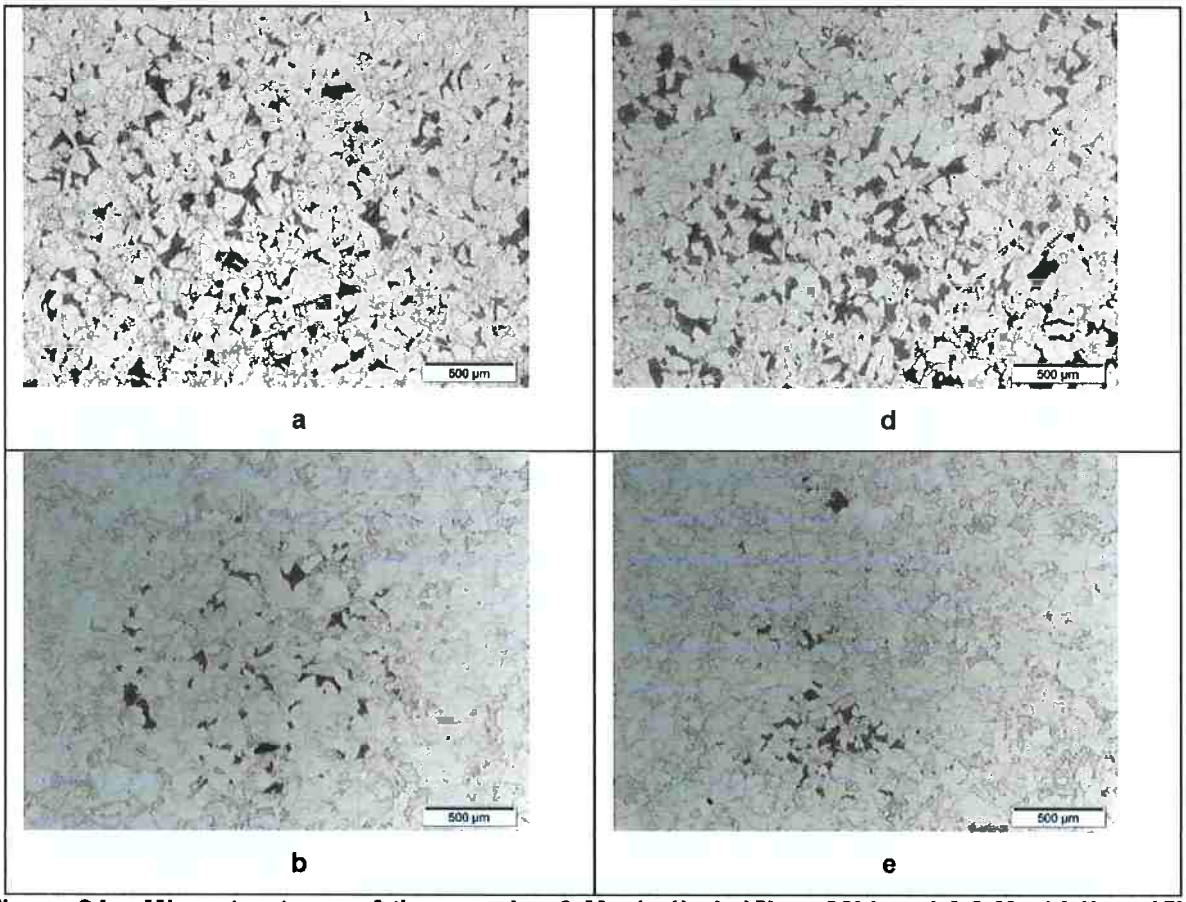

Figure 24 – Microstructures of the samples 0 Mo (a.1h, b.15h, c.30h) and 0,2 Mo (d.1h, e.15h, f.30h) during isothermal holding at 675 °C, near the center.

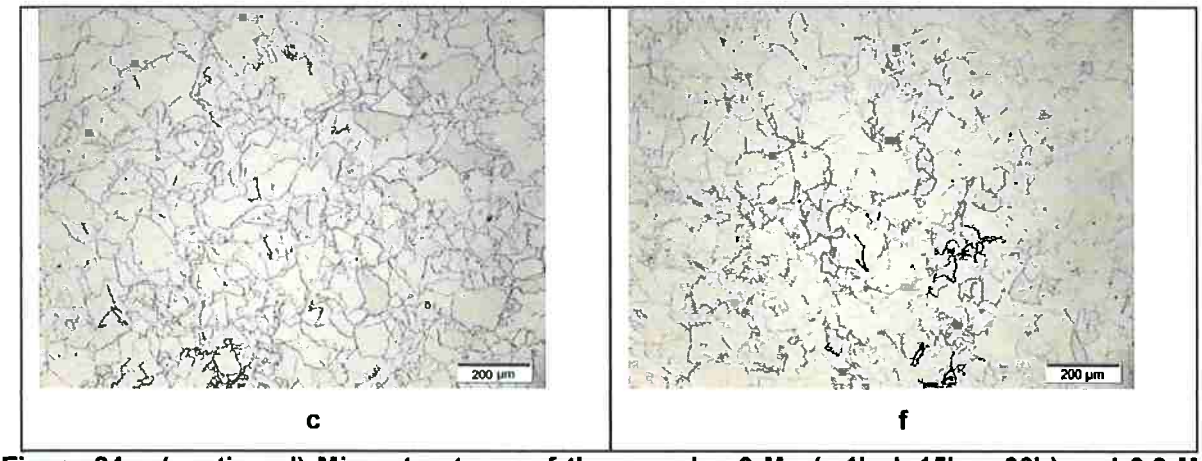

Figure 24 – (continued) Microstructures of the samples 0 Mo (a.1h, b.15h, c.30h) and 0,2 Mo (d.1h, e.15h, f.30h) during isothermal holding at 675 °C, near the center.

In order to avoid decarburization, it was decided to nickel-coat the samples. The result of this procedure can be seen in Figure 25, which shows a comparison between a 0,2 Mo sample without Ni-coating and another with Ni-coating which were tested at 675 °C for 15h.

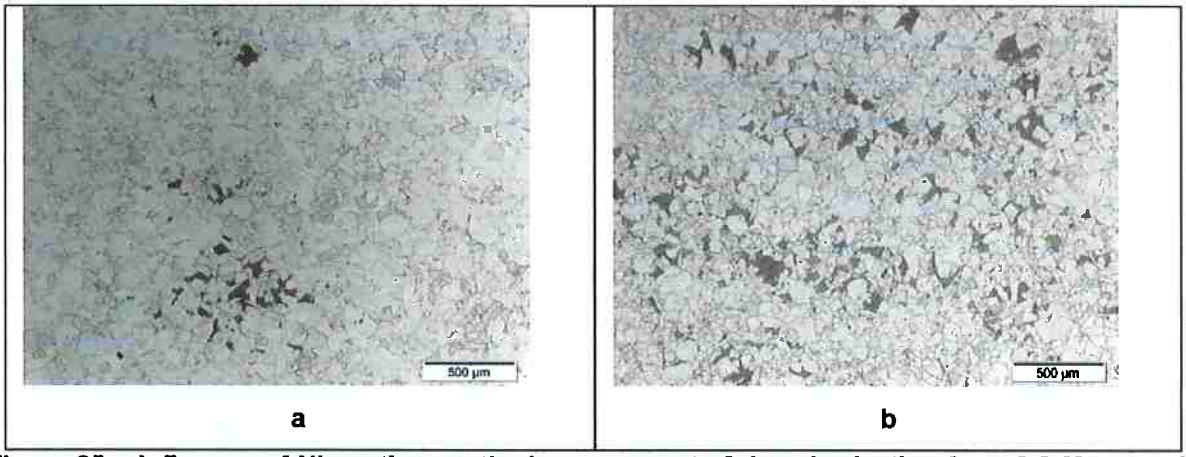

Figure 25 – Influence of Ni-coating on the improvement of decarburization for a 0,2 Mo sample submitted to a isothermal holding at 675 °C for 15h: (a) no Ni-coating, (b) with Ni-coating.

V.2.2. Kinetics

Figure 26 presents the results obtained on the dilatometer for a 1-hour analysis at 675 °C for 0 Mo, 0,2 Mo and 0,4 Mo samples. For better representation, the beginning of the transformation in Figure 26a was placed at the same time. By observing Figure 26a, it can be noticed that the addition of Mo makes the transformation slower, that is, Mo slows down the transformation of ferrite, the

formation of the carbides and any other reaction that might be taking place as these transformations take more time to take place. This result may come from the fact that MoC has a high solubility in austenite [Pavlina 2012]. This difference is even bigger when we see the results of the 0,4 Mo sample. Figure 26b shows also that Mo slows down this transformation, but after further transformation. This phenomenon of the delay of the transformation happens until approximately 1950 s, as it can be seen in Figure 26b. After this time, the curve of 0,4 Mo sample overpasses the one of 0,2 Mo, indicating volumetric expansion probably due to the formation of the precipitates (Nb and Mo carbides or carbonitrides). After 30 minutes almost all ferrite is formed and at 1h the transformation seems to be finished for all alloys.

This result that Mo slows the transformation of ferrite is in agreement with the literature. In the work of *Yu et al.*, it was seen that there is a strong delay of γ/α transformation [Yu 2013].

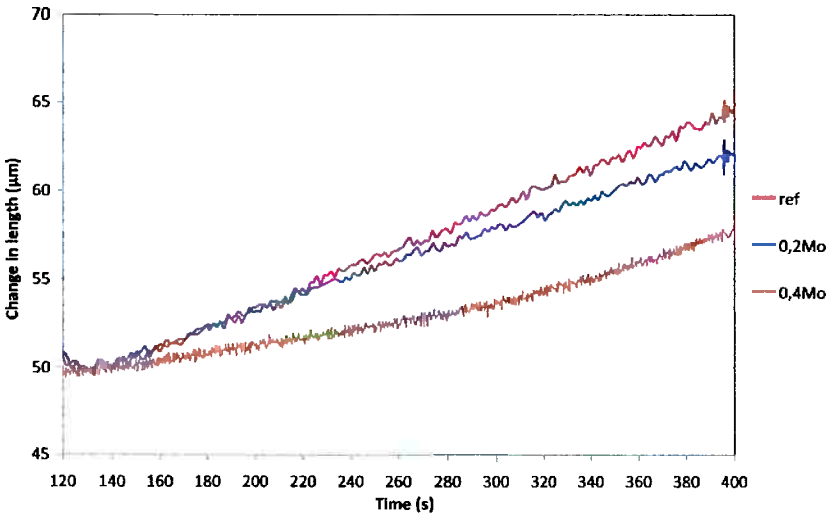

(a)

Figure 26 – Results obtained from the dilatometer representing change in length *versus* time during isothermal treatment showing the progression of the transformation: (a) Mo addition induces the reduction of the transformation, (b) After thirty minutes, almost all transformation is complete.

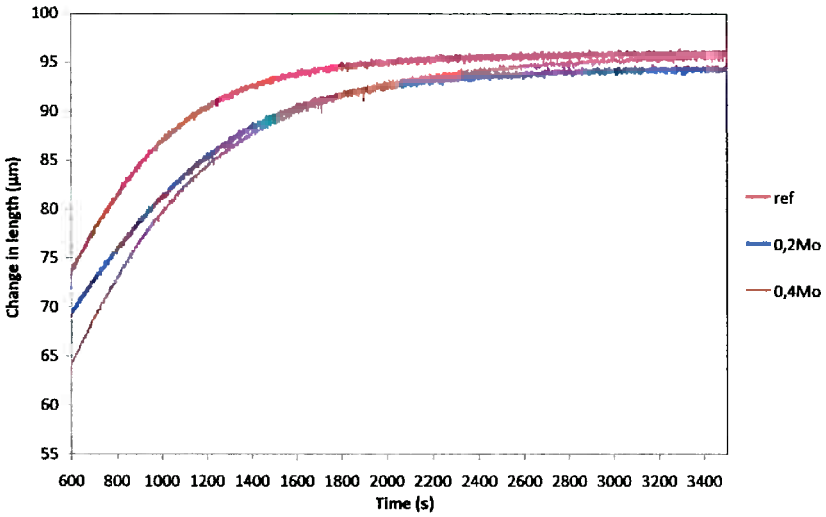

(b)

Figure 26 – (continued) Results obtained from the dilatometer representing change in length *versus* time during isothermal treatment showing the progression of the transformation: (a) Mo addition induces the reduction of the transformation, (b) After thirty minutes, almost all transformation is complete.

V.2.3. Micro-hardness

Micro-hardness tests were done in 0 Mo and in 0,2 Mo samples treated for 15h at 675 °C, in order to better understand the microstructures obtained. Three different microstructures shown in Figure 27, designed by A, B, and C, could be distinguished and their hardness was measured, results displayed in Table 3.

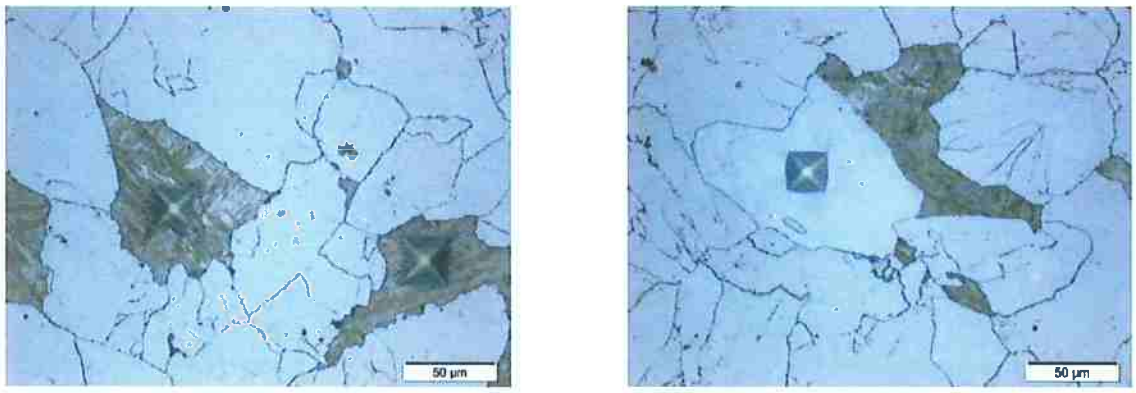

(a) (b)

Figure 27 – Example of the micro-hardness measurements made in microstructures designed by (a) A, (b) B and (c) C.

(c)

Figure 27 – (continued) Example of the micro-hardness measurements made in microstructures designed by (a) A, (b) B and (c) C.

Table 3 - Micro-hardness results.

Microstructures	A	B	C
0 Mo _ 15h	507 HV	189 HV	172 HV
0,2 Mo _ 15h	480 HV	190 HV	200 HV

Through the results obtained in Table 3 and by observation of the microstructures, examples in Figure 27, the microstructures were characterized as follows:

A) Martensite;

B) Decarburized austenite;

C) Ferrite.

V.2.4. Samples characterization

Figure 28 shows the micrograph of the 0 Mo sample passed through 1-hour cycle, quenched and then again at 1-hour cycle at 675 °C. Micrographs of 0 Mo and 0,2 Mo samples tested for 1h and for 15h at 675 °C are shown in Figure 24.

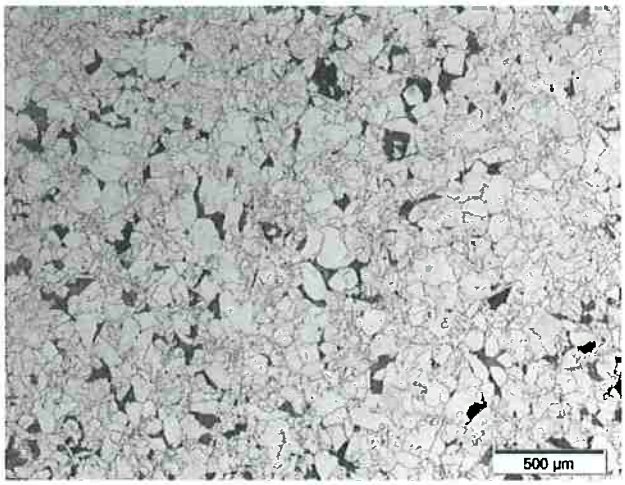

Figure 28 - Micrograph of the 0 Mo sample passed through a 1-hour heat treatment at 675 °C, quenched and then reheated to 675 °C for another 1h.

The SEM images of the 0 Mo sample passed through a 1-hour heat treatment at 675 °C, quenched and then reheated to 675 °C for another 1h can be seen in Figure 29. Austenite transformed into martensite after the first quench be seen in Figure 29a. Figure 29b presents a closer look into the microstructure and it can be observed that, after being reheated at 675°C, a second phase appears. At this temperature this phase is more likely to be cementite. In order to better analyze the microstructures, a Thermocalc® analysis (with TCFE database) was made, which can be seen in Annex 2.

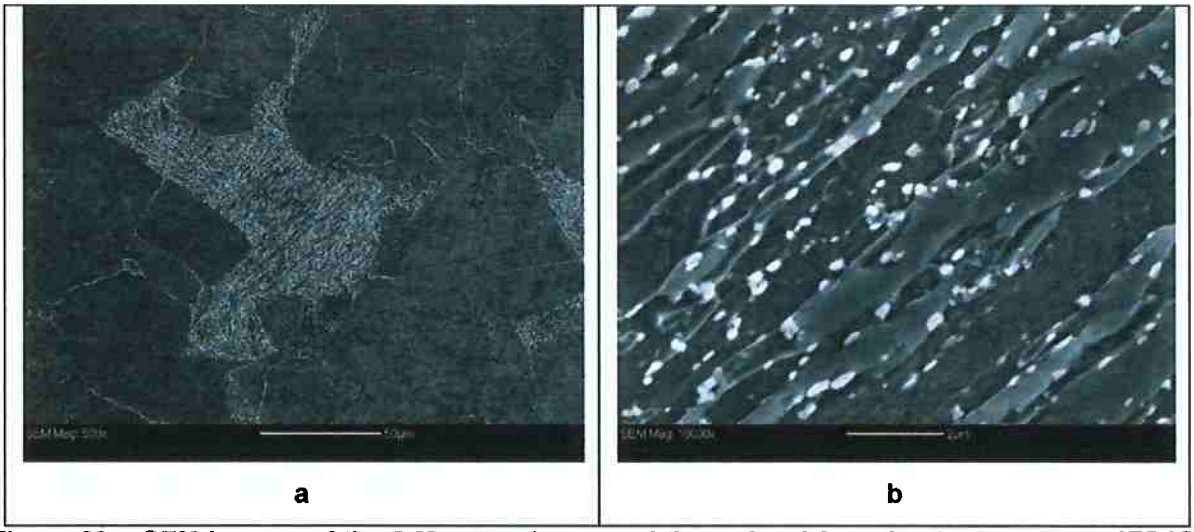

Figure 29 – SEM images of the 0 Mo sample passed through a 1-hour heat treatment at 675 °C, quenched and then reheated to 675 °C for another 1h.

The micrographs of the samples submitted to a 72 hour-heat treatment at 675 °C can be seen in Figure 30.

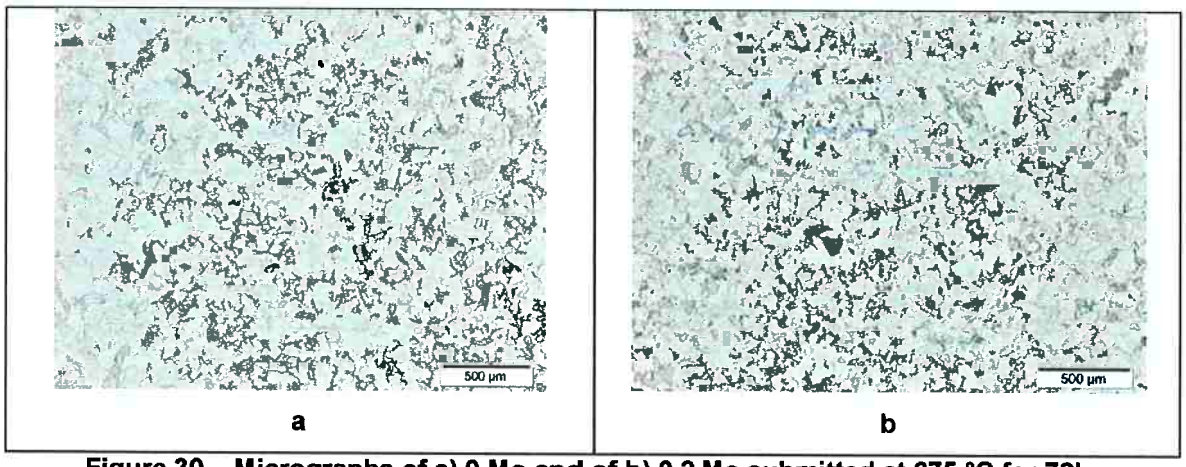

Figure 30 – Micrographs of a) 0 Mo and of b) 0,2 Mo submitted at 675 °C for 72h.

Figure 31 shows the SEM images of the 0,2 Mo sample treated for 72 hours at 675 °C. Its microstructure is unknown, but it can be seen that precipitation was formed inside it.

Figure 31 - SEM images of the 0,2 Mo sample treated for 72 hours at 675 °C.

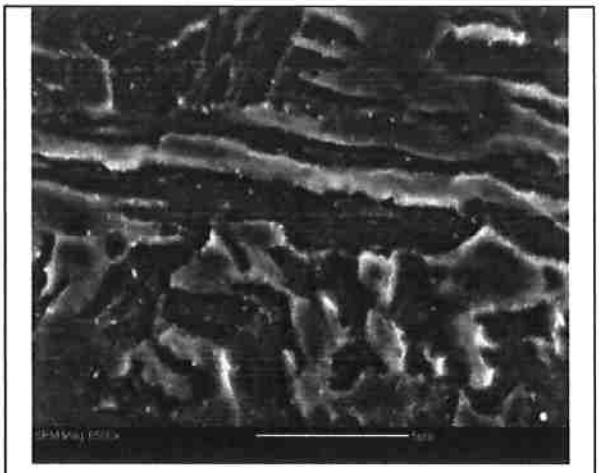

c

Figure 31 – (continued) SEM images of the 0,2 Mo sample treated for 72 hours at 675 °C.

V.2.5. Precipitates characterization

The TEM images taken from the replicas of the 0 Mo samples can be seen in Figure 32.

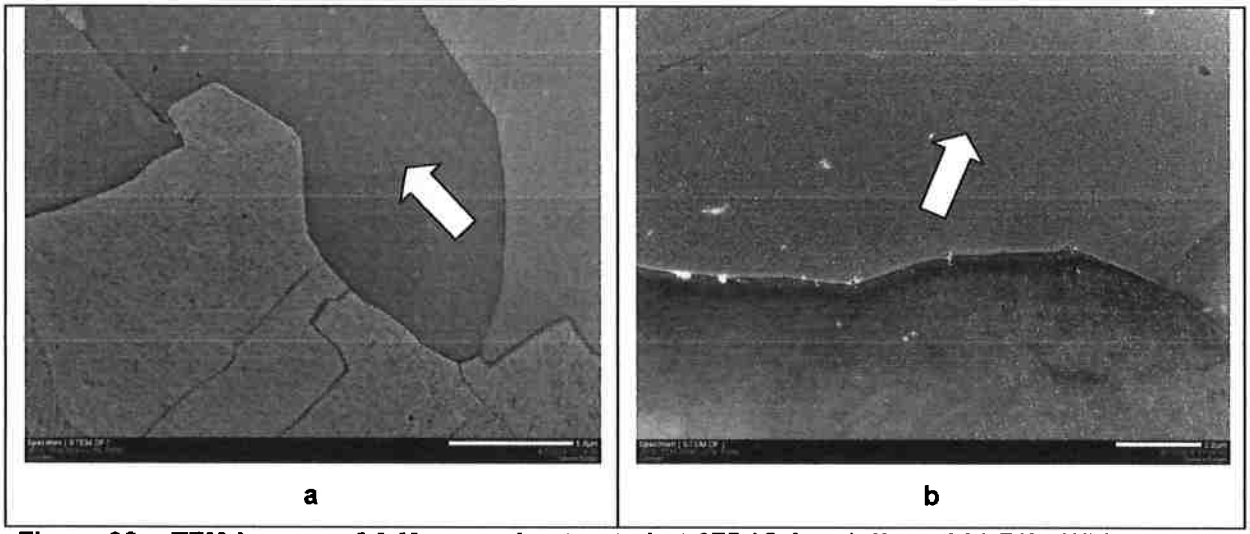

a b

Figure 32 – TEM images of 0 Mo samples treated at 675 °C for a) 1h and b) 72h. White arrows indicate the ferritic region analyzed.

The TEM images taken from the replicas of the 0,2 Mo samples can be seen in Figure 33.

It should be mentioned that the precipitates were taken always from the ferritic regions indicated by white arrows in Figure 32 and Figure 33, that is, it was

never taken the precipitates from the regions shown in Figure 29b and from Figure 31b and c.

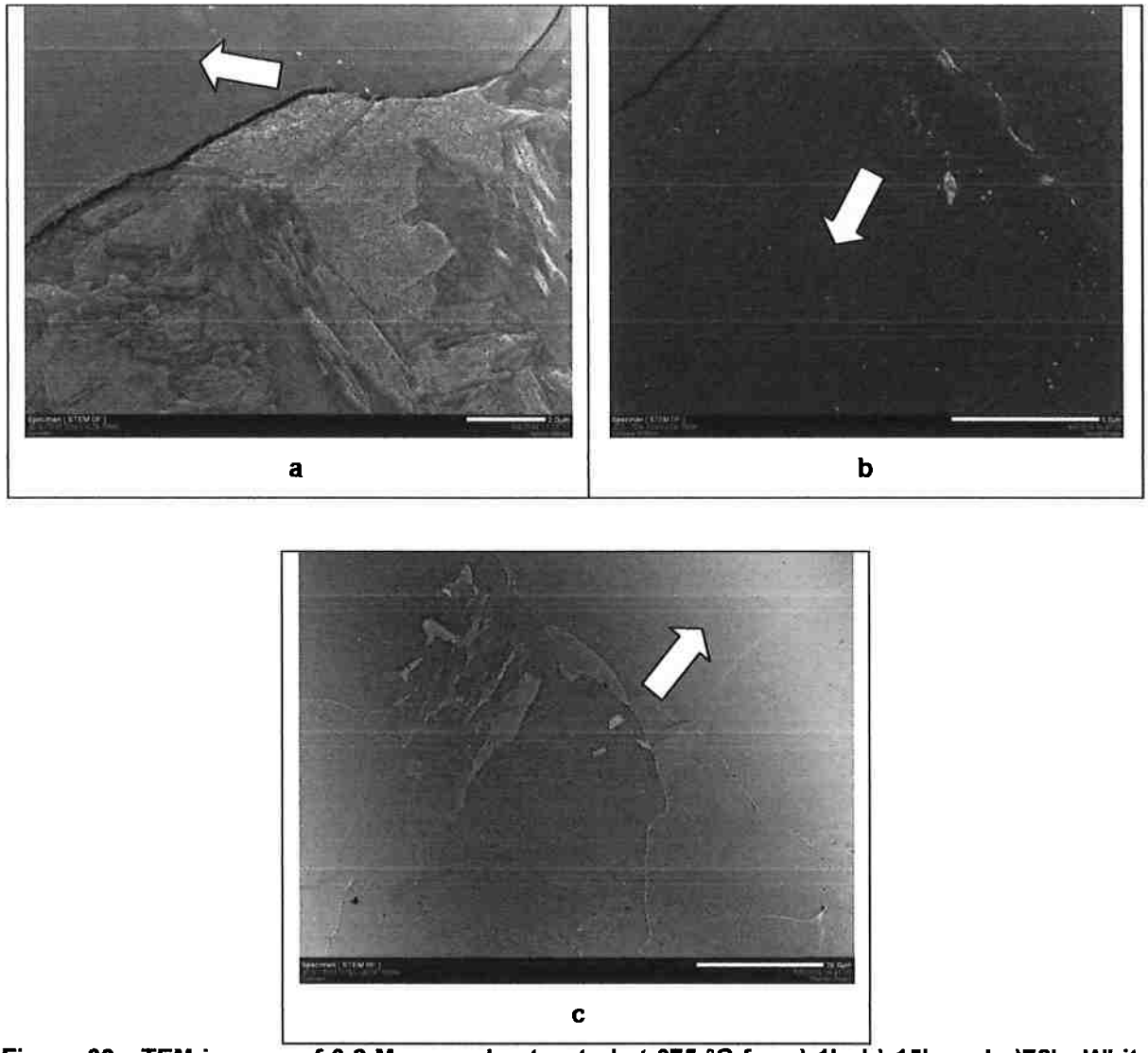

Figure 33 - TEM images of 0,2 Mo samples treated at 675 °C for a) 1h, b) 15h and c)72h. White arrows indicate the ferritic region analyzed.

V.2.6. Precipitates evolution

Figure 34 presents the precipitates evolution of 0 Mo and 0,2 Mo samples treated at 675 °C for 1h, 15h and 72h.

Growth is observed as a function of time. At the longest time, precipitates have clearly a plate form, as seen in Figure 34c and f.

The Aphelion® software was used to study the precipitates size and one example of its analysis can be seen in Figure 35. Table 4 shows the number of

precipitates analyzed in each case of heat-treatment at 675 °C for 1h, 15h and 72h for 0 Mo and 0,2 Mo samples. As the samples have a plate-form after the 72 hour-treatment, it was difficult to study the thickness as the position of the precipitates varies in the replicas. Because of this, only the lengthening was taken into account.

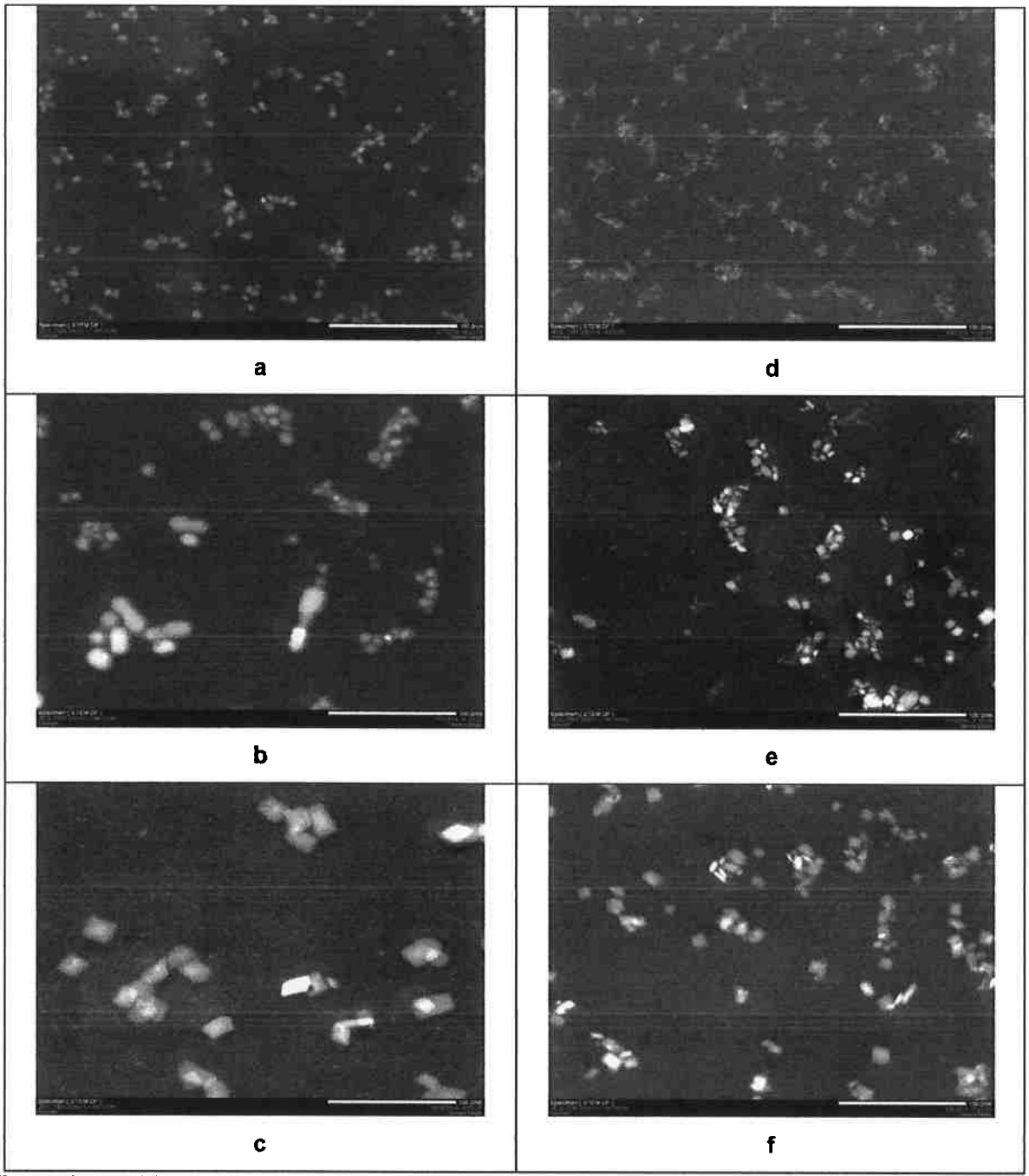

Figure 34 – TEM images of the replicas showing the precipitates of 0 Mo (a.1h, b.15h, c.72h) and 0,2 Mo (d.1h, e.15h, f.72h) samples during isothermal holding at 675 °C.

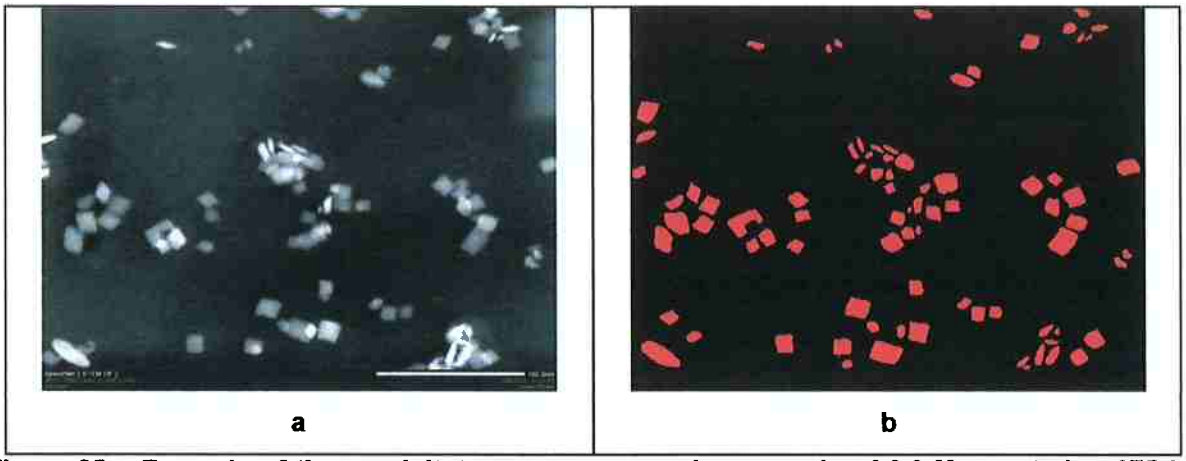

Figure 35 – Example of the precipitates measurement in a sample of 0,2 Mo treated at 675 °C for 72h.

Table 4 – Number of precipitates analyzed in each case for a heat-treatment at 675 °C.

	0 Mo	0,2 Mo
1h	519	693
15h	490	897
72h	95	521

The results of the measurement of the precipitates can be seen in the form of histograms in Figure 36.

Table 5 shows the length of the precipitates as a function of time and composition and these results are compared in Figure 37.

The preliminary results show that Mo reduces the lengthening of the precipitates. This is not clear for the shortest time, but it becomes clear after 15h.

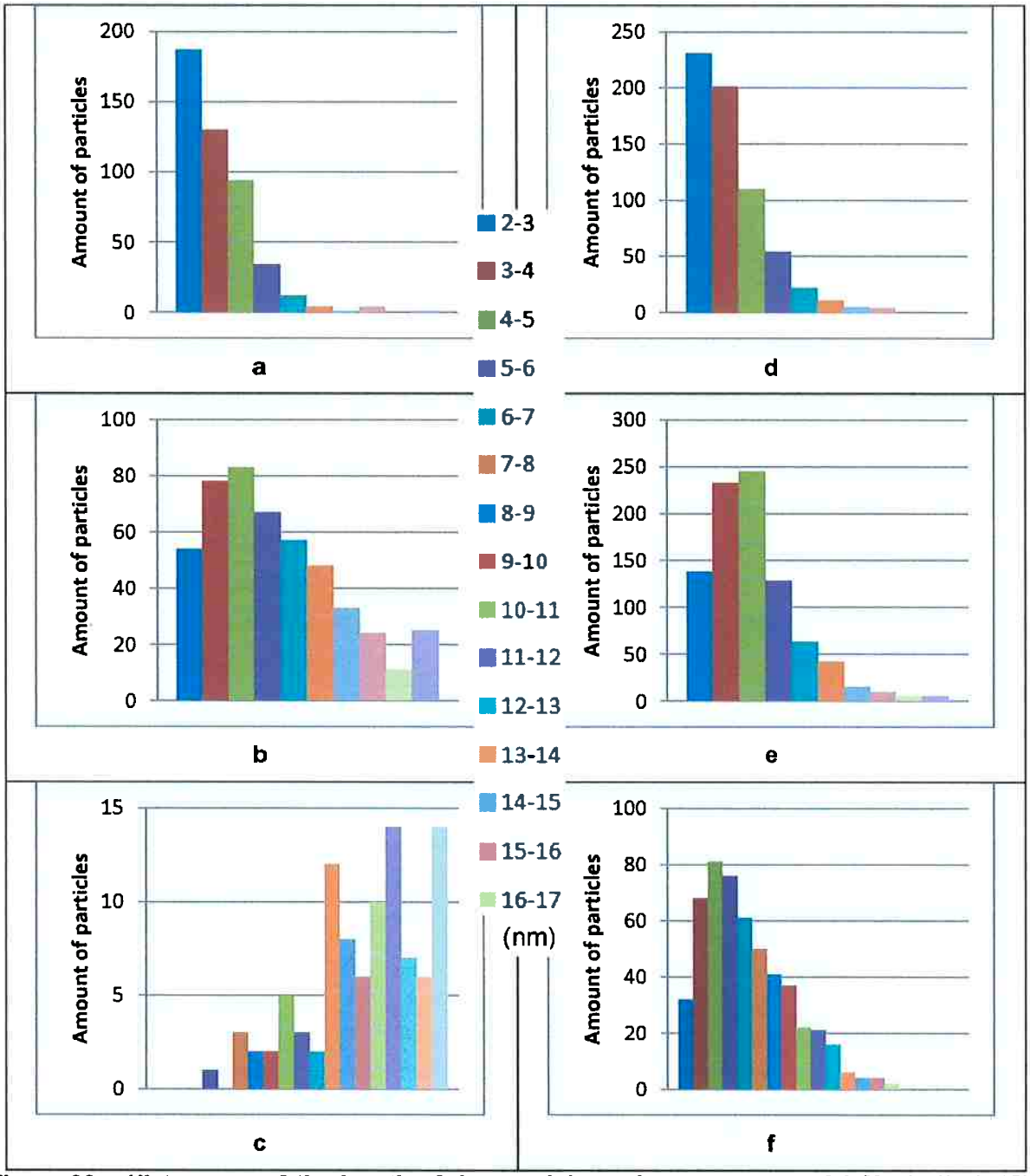

Figure 36 – Histograms of the length of the precipitates in nanometers of 0 Mo (a.1h, b.15h, c.72h) and 0,2 Mo (d.1h, e.15h, f.72h) samples during isothermal holding at 675 °C.

Table 5 – Lengthening of the precipitates, in nanometers, as a function of time and composition.

(nm)	0 Mo	0,2 Mo
1h	3,4 ± 1,4	3,6 ± 1,4
15h	5,8 ± 2,8	4,5 ± 1,7
72h	15,9 ± 4,0	6,7 ± 3,0

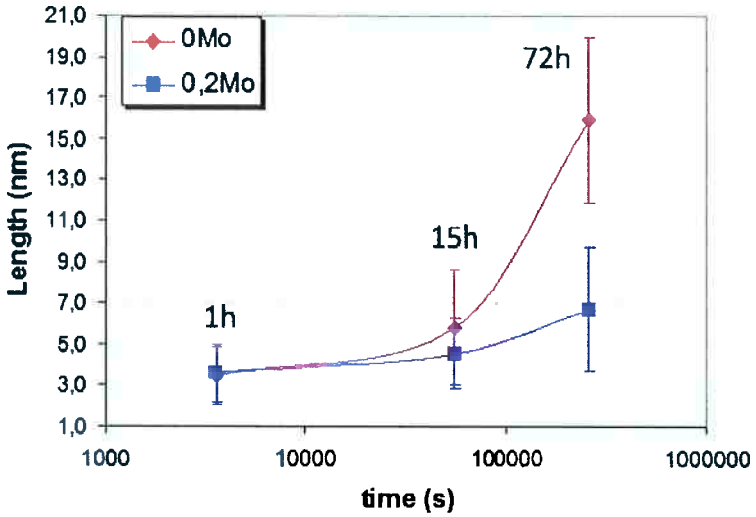

Figure 37 – Length of the precipitates as a function of time and composition.

Mo reduces the size of the carbide precipitates and also retards their coarsening behavior. This is according to the literature as it was said that Mo slows the incorporation of Nb into the carbonitride and reduce the interfacial energy, thus reducing the coarsening rate.

VI. Conclusions

The results obtained allow some conclusions:

a) Mo slows down the formation of ferrite;
b) Mo retards the growth of precipitates, as it was seen, it reduces the lengthening of the precipitates.

It is not stated in this report whether the precipitates measured come from Nb or from Mo. To have so, it should have been done an elemental mapping via EDS in TEM.

As there is not this result, it might be discussed the stability of both carbides. As seen in Figure 14, the solubility of both carbides is presented and it can be seen that Mo is a few orders of magnitude more soluble than Nb, that is, Nb carbides/carbonitrides are more stable than Mo carbides. A high solubility in austenite suggests that incorporation of Mo into complex carbonitride precipitates formed in austenite is negatively affected, which may explain the delay of ferrite formation.

The stability of both carbides can also be studied in a relation with the melting point. Nb_2C presents a melting point of 3100 °C while Mo_2C, 2410 °C, which also shows that Nb carbide is more stable than Mo carbide. The crystal structure also can be useful to predict the stability of the carbides. NbC-Nb_4C_3 is cubic, while Mo_2C-MoC is hexagonal. Simple structures are more stable which also shows the greater stability of Nb carbides/carbonitrides than Mo carbides [Tschiptschin 1988].

At this work, there are evidences that Mo may reduce the coarsening rate as it retards the growth of precipitates. Mo is believed to suppress precipitation and especially coarsening of NbC. To better understand its influence on coarsening, a volume fraction study of the precipitates should be done.

The plate-shape form of precipitates is better for precipitate hardening since it impedes the movement of dislocations better than spherical precipitates.

REFERENCES

[Altuna 2009]
M. A. Altuna, A. Iza-Mendia, I. Gutierrez, **Precipitation Strengthening produced by the formation in ferrite of Nb carbides**, La Metallurgia Italiana, (2009), pp.41-47.

[Altuna 2012]
M. A. Altuna, A. Iza-Mendia, I. Gutierrez, **Precipitation of Nb in ferrite after austenite conditioning. Part II: Strengthening contribution in High-Strength Low-Alloy (HSLA) Steels**, Metallurgical and Materials Transactions A, Vol.43, (2012), pp.4571-4586.

[Bhadeshia 2000]
H. K. D. H. Bhadeshia, **Course of Materials Science & Metallurgy**, University of Cambridge, (2000).

[Bhattacharya 1972]
S. K. Bhattacharya and K. C. Russell, **Activation Energies for the Coarsening of Compound Precipitates**, Metall. Trans., Vol. 3, (1972), p.2195.

[Burke 1965]
J. Burke, **Theory of diffusional growth processes**, in The kinetics of phase transformations in metals, (1965), p.152.

[Calphad]
Computational Thermodynamics <http://www.calphad.com/iron-molybdenum.html> (last view on 02/12/2014).

[Central Microscopy]
Central Microscopy of the University of Iowa
<http://cmrf.research.uiowa.edu/transmission-electron-microscopy> (last view on 12/09/2014).

[Enloe 2012]
C. M. Enloe, K. O. Findley, C. M. Parish, M. K. Miller, B. C. De Cooman and J. G. Speer, **Compositional evolution of microalloy carbonitrides in a Mo-bearing microalloyed steel**, Scripta Materialia, (2012), p.55.

[Furuhara 2008]
T. Furuhara, K. Kikumoto, H. Saito, T. Sekine, T. Ogawa, S. Morito and T. Maki, **Phase transformation from fine-grained austenite**, ISIJ Int., Vol. 48, (2008), pp. 1038-1045.

[García de Andrés 2003]
C. García de Andrés, F. G. Caballero, C. Capdevila and D. San Martín, **Revealing austenite grain boundaries by thermal etching: advantages and disadvantages**, Materials Characterization, Vol. 49, (2003), p.121.

[Goldstein 2003]
J. Goldstein, **Scanning electron microscopy and x-ray microanalysis**, Kluwer Academic/Plenum Publishers, (2003), p.689.

[Greenwood 1969]
G. W. Greenwood, **Particle Coarsening**, in The mechanism of phase transformations in crystalline solids, Institute of Metals, London, (1969), p.103.

[Hulka]
K. Hulka, C. Klinkenberg and J. Patel, **Hot Rolled HSLA strip steels for automotive and construction applications**, NIOBIUM Products Company GmbH, p.2.

[Jia-ling 1988]
L. Jia-ling et W. Mu-bing, **Effect of Mn on Yield Behavior of Dual-Phase Steel**, in Proc. Conf. 'Thermec-88', The Iron and Steel Inst. of Japan, (1988), p.699.

[Keown 1985]
S.R. Keown and J.H. Woodhead, **The history of microalloyed steels**, in HSLA Steels: Metallurgy and Applications, eds. J.M. Gray, T. Ko, Z. Shouhua, W. Baorong and X. Xishan, The Chinese Society of Metals China Science and Technology Exchange Center, ASM International, (1985), pp.15-28.

[Klinkenberg 2007]
C. Klinkenberg, **Niobium in Microalloyed Structural & Engineering Steel**, Materials Science Forum, Vol.4261, (2007), pp.539-543.

[Köver 2012]
M. Köver, **Analysis of phase transformations in selected low-alloy steels by thermal and computational methods**, Diploma Thesis, Faculty of Materials Science and Technology in Trnava, (2012).

[Lechuk 2000]
S. J. Lechuk, **A study of austenite grain growth in a Ti-Nb HSLA steel**, Master Thesis, The University of British Columbia, (2000).

[Lee 2002]
W. B. Lee, S. G. Hong, C. G. Park, K. H. Kim and S. H. Park, **Carbide Precipitation and High-Temperature Strength of Hot-rolled High-Strength, Low-Alloy Steels Containing Nb and Mo**, Metallurgical and Materials Transactions, Vol.33A, (2002), p.319.

[Martin 1997]
J. W. Martin, R. D. Doherty and B. Cantor, **Precipitate coarsening: 'Ostwald ripening'**, in Stability of microstructure in metallic systems, Cambridge University Press, Cambridge, (1997), p.239.

[Microscope Master]
The Complete Microscope Guide
<http://www.microscopemaster.com/transmission-electron-microscope.html> (last view on 12/09/2014).

[NanoScience]
NanoScience Instruments
<http://www.nanoscience.com/products/sem/technology-overview/how-sem-works/>
(last view on 12/09/2014).

[Netzch 2005]
Operating Instructions High Temperature Dilatometer DIL 402 C/7, Netzch, (2005), pp.35-57.

[Park 1991]
S.-H. Park, **Modelling and Measurement of the Continuous-Cooling-Precipitation Kinetics of Nb(CN) in HSLA Steels**, PhD Thesis, McGill University, (1991), pp.11-13.

[Park 2013]
D.-B. Park, M.-Y. Huh, J.-H. Shim, J.-Y. Suh, K.-H. Lee and W.-S. Jung, **Strengthening mechanism of hot rolled Ti and Nb microalloyed HSLA steels containing Mo and W with various coiling temperature**, Materials Science & Engineering A, Vol.560, (2013), p.528.

[Pavlina 2012]
E. J. Pavlina, J. G. Speer and C. J. Van Tyne, **Equilibrium solubility products of molybdenum carbide and tungsten carbide in iron**, Scripta Materialia, Vol. 66, (2012), p.243.

[Pickering 1992]
F.B. Pickering, **High Strength Low Alloy Steels**, in Materials Science and Technology: a comprehensive treatment ,eds. R.W. Cahn, P.Haasen, E.J. Kramer, VCH, Vol.7, (1992), pp.335-399.

[Rösler 2006]
J. Rösler, H. Harders and M. Bäker, **The structure of materials**, in Mechanical Behaviour of Engineering Materials, Springer, Heidelberg (2006), pp.15-16.

[Serafim da Silva 2013]
C. Serafim da Silva, **Influence of processing parameters on microstructural evolution in a HSLA steel,** Rapport de stage de 5ème année, ArcelorMittal Global R&D Maizières, (2013), p.31.

[Speich 1965]
G. R. Speich and R. A. Oriani, **The rate of coarsening of copper precipitate in an alpha-iron matrix**, Transactions of the Metallurgical Society of Aime, Vol. 23, (1965), p.623.

[Stahl-Eisen 1998]
Guidelines for preparation, execution and evaluation of dilatometric transformation tests on iron alloys, STAHL-EISEN-Prüfblätter, Vereins Deutscher Eisenhüttenleute, Vol. 1681, (1998), pp.1-10.

[Takahashi 1989]
M. Takahashi, H. K. D. H. Bhadeshia, **The interpretation of dilatometric data for transformations in steels**, Journal of Materials Science, Vol. 8, (1989), pp.477-478.

[Tariq 2010]
F. Tariq, **Evaluation of microstructure and mechanical properties during quenching and tempering of ultrahigh strength 0.3C Si-Mn-Cr-Mo low alloy steel**, Journal of Materials Science, Vol. 45, (2010), pp.1695-1708.

[Tschiptschin 1988]
A. P. Tschiptschin, H. Goldenstein, A. Sinatora, **Metalografia dos Aços**, Associação Brasileira de Metais – ABM, (1988), pp.178-180.

[Wagner 2001]
R. Wagner, R. Kampmann and P. W. Voorhees, **Homogeneous Second-phase precipitation**, in Phase Transformations in Materials, WILEY-VCH Verlag GmbH, Weinheim, (2001), p.310.

[Yu 2013]
Y. J. Yu, D. S. Park, H. S. Noh, J. M. Kim, K. J. Lee, **Effect of Nb and Mo on the austenite decomposition in low carbon steels**, Hanyang University, (2013).

ANNEX 1 – COMPLETE COMPOSITION OF THE SAMPLES.

(wt%)	C	Nb	Mo	Cr	Mn	Al	Ti	N	Si	P	S	Cu	Ni	B	V
0 Mo	0,0530	0,1000	0,0048	0,0140	1,5000	0,0220	0,0029	0,0015	0,0100	0,0024	0,0013	0,0083	0,0066	0,0001	0,0040
0,1 Mo	0,0550	0,1100	0,1200	0,0130	1,5000	0,0250	0,0026	0,0016	0,0097	0,0023	0,0027	0,0099	0,0068	0,0001	0,0046
0,2 Mo	0,0560	0,1000	0,2100	0,0130	1,5000	0,0200	0,0030	0,0017	0,0130	0,0026	0,0027	0,0100	0,0068	0,0001	0,0045
0,4 Mo	0,0550	0,1100	0,4000	0,0200	1,5418	0,0308	0,0048	0,0033	0,0490	0,0044	0,0022	0,0150	0,0065	0,0003	-

ANNEX 2 – THERMOCALC® RESULTS.

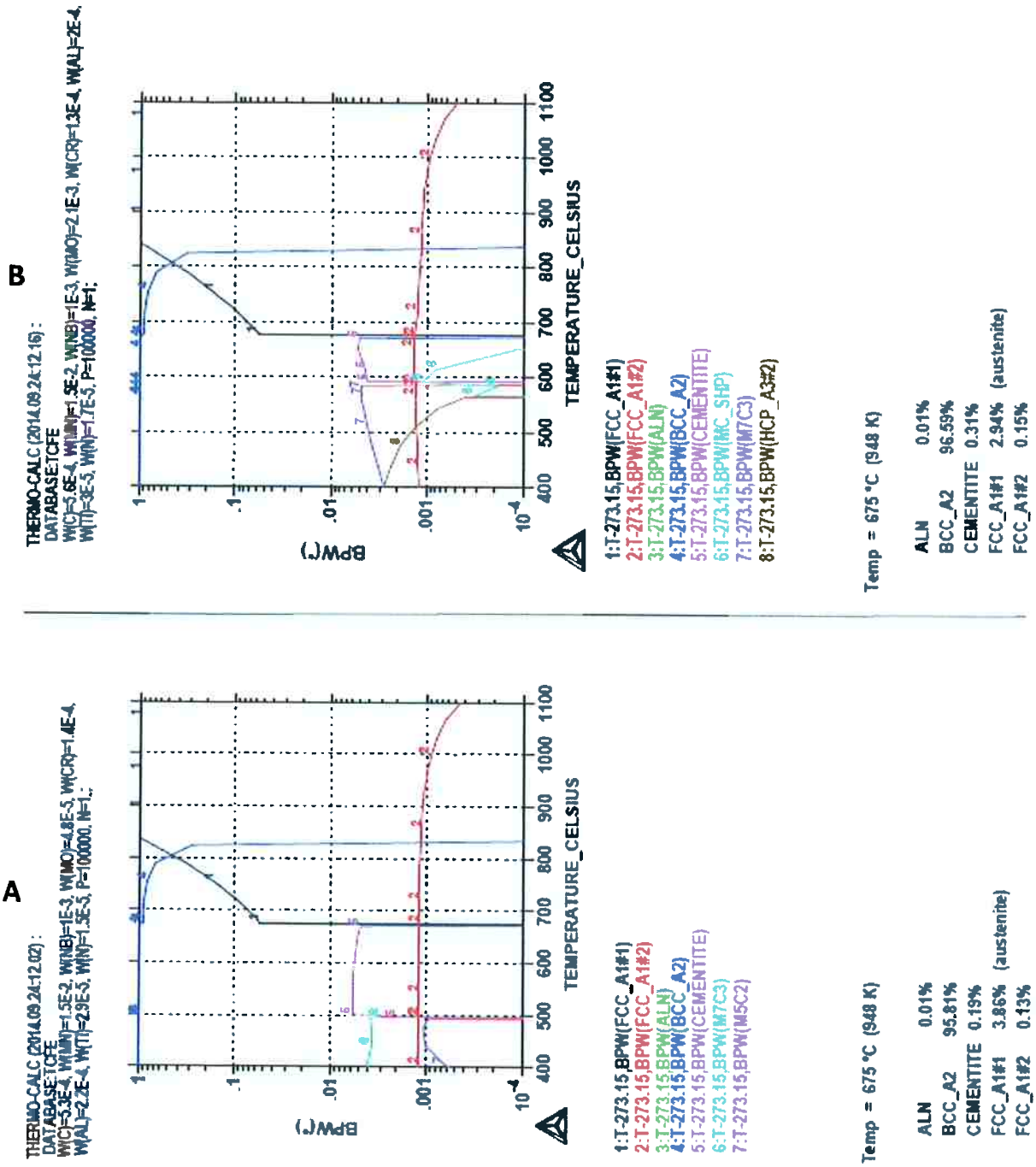

A) 0 Mo sample

B) 0,2 Mo sample